



Synthesis of a novel green biopolymer-based composites beads for removal of methylene blue from aquatic medium: isotherm, thermodynamic and kinetic investigation

Şerife Parlayıcı¹ · Aslı Aras¹

Received: 2 October 2023 / Revised: 8 January 2024 / Accepted: 17 January 2024 /

Published online: 15 February 2024

© The Author(s) 2024

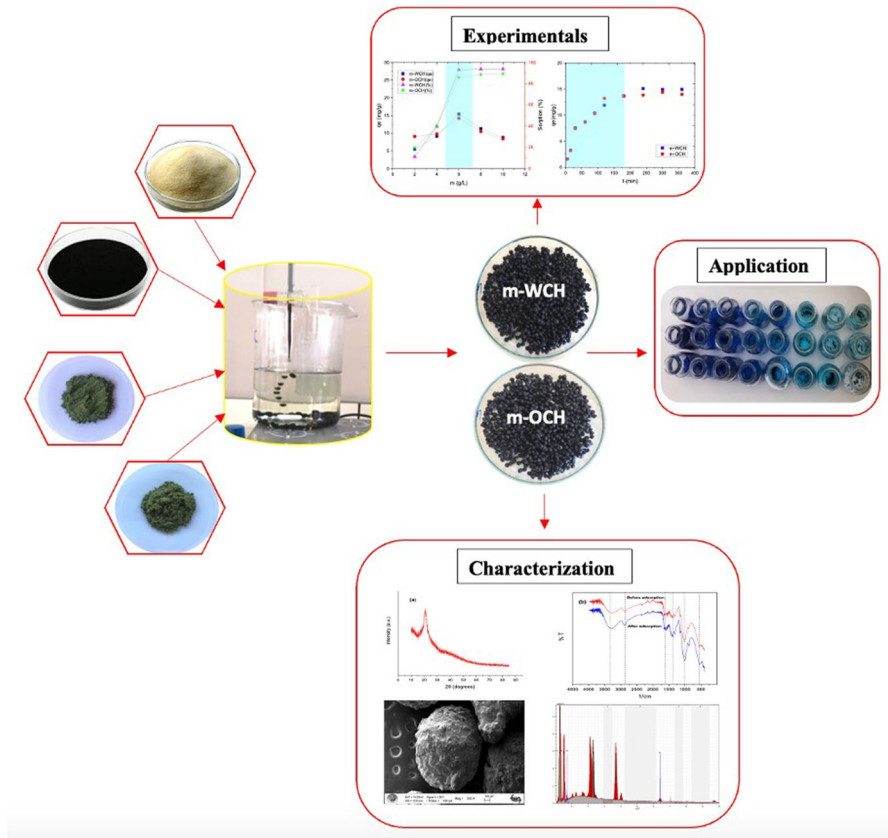
Abstract

The increase in the world population and the decrease in clean water resources increase people's interest in water purification technologies. Many industries, such as the textile industry, leather industry, cosmetics and food industry, color their products with substances such as dyes and pigments. In this study, a cheap, useful, innovative, environmentally friendly, and sustainable adsorbent was developed for the removal of Methylene Blue (MB), one of the dyes that is harmful to the environment. In fruit tree cultivation, in addition to the product, very high amounts of by-products/waste (branches, bark, leaves, fruit seeds, fruit shells, etc.) are produced. In this direction, walnut tree and olive tree wastes were immobilized with chitosan, made magnetic (m-WCH and m-OCH), and the adsorption of MB on the developed adsorbents was examined in a batch system. Characterization of the synthesized biocomposite adsorbents was performed by FT-IR, SEM, EDX and XRD analyzes. It has been thoroughly described how the pH solution of the MB dye compares to the pH_{PZC} of the adsorbent surface. The pH_{PZC} values for m-WCH and m-OCH were 5.2 and 5.5 respectively. MB adsorption of biocomposites depends on the pH of the environment (3–8), amount of adsorbent (2–10 $g L^{-1}$), contact time (5–360 min), temperature (25–55 °C) and initial dye concentration (10–250 ppm) was examined as a function. The obtained data were evaluated with kinetic and isotherm models. Using adsorption equilibrium data obtained from MB adsorption studies using m-WCH and m-OCH biocomposite adsorbents, their suitability to Langmuir, Freundlich, Stachard, Dubinin–Radushkevich and Temkin models was examined. The empirical data of MB adsorption by m-WCH and m-OCH showed agreement with the Langmuir isotherm model. The maximum adsorption capacity for MB by m-WCH and m-OCH was estimated to be 85.47 $mg g^{-1}$ and 53.48 $mg g^{-1}$, respectively. The result showed that a higher adsorption selectivity on m-WCH compares to m-OCH. Among the kinetic models applied, the pseudo-second-order kinetic model was identified with the highest regression coefficients. In the light of these results, it was determined that there are new promising adsorbents of natural origin,

Extended author information available on the last page of the article

with higher adsorption capacity, lower cost, and alternatives to commercially used adsorbents in the removal of MB from aqueous media.

Graphical abstract



Keywords Biowaste · Chitosan · Nano Fe_3O_4 · Methylene blue · Adsorption

Introduction

The rapid growth of the industry produces positive results by quickly meeting people's needs and supporting economic development. However, it also brings environmental pollution. It is estimated that approximately 10–15% of textiles are discharged into wastewater after dyeing [1]. Nearly 10,000 textile colors are sold annually [2]. It is known that textile industry wastewater has a high volume and a complex structure depending on the chemicals and dyestuffs used [3]. In addition, considering that even small amounts of dyestuffs create pollution in a large water

environment, it can be understood that these wastewaters, which have a high color load and are difficult to biodegrade, will be very difficult to purify through natural processes or will take a long time. Besides visible pollution, it can negatively affect biological cycles, especially photosynthesis processes, by blocking the penetration of light through deep water bodies. This toxic property and possible carcinogenic effects of dyes pose a great threat to the environment by negatively affecting biological cycles and ecosystems. Purification of these carcinogenic dyes from wastewater is an important environmental problem [4].

One of the most consumed materials in the dye industry is MB, which is widely used for coloring in the silk, wool, cotton, paper, leather and plastic industries [5]. However, with the release of partially or untreated MB dye laden wastewater from any of the above-mentioned industries, aquatic fauna, beneficial microbes and human life are threatened. One of the reasons for this is the significant toxicity of dyes such as MB at high concentrations [6]. The chemical formula of MB (basic blue 9), a cationic dye, is $C_{16}H_{18}ClN_3S \cdot 3H_2O$ and its molecular weight is $373.90 \text{ g mol}^{-1}$. MB dye is harmful to human health above a certain concentration due to its significant toxicity [7]. Exposure to MB may cause eye burns, and if swallowed, may cause diarrhea and nausea. Continuous contact with MB concentrated solutions has been reported to have a negative effect on the ability of sperm to move more efficiently in human reproduction [8]. Skin contact may cause skin redness, itching, or skin necrosis. Additionally, when inhaled for a long time, it causes diseases such as methemoglobinemia, cyanosis (bruising disease), convulsion (convulsion disease), and dyspnea (shortness of breath) [9]. Due to the characteristic stability of the aromatic ring in the molecular structure of MB, it is toxic, carcinogenic, non-biodegradable and can pose a serious threat to human health and cause devastating effects on the environment [6, 10]. This chemical compound has been reported to be teratogenic and embryotoxic. Toxic effects were confirmed in a study in which MB was exposed to angelfish and rats, respectively [11]. At the same time, MB generally has a high molar absorption coefficient ($664 \text{ nm}^2/\text{de}$, $\sim 8,4 \times 10^4 \text{ L mol}^{-1} \text{ cm}^{-1}$), which can cause the weakening of sunlight transmittance and therefore reduce oxygen solubility, affecting the biological community [12, 13].

Along with water pollution, water scarcity, climate change and decrease in biodiversity show the necessity of industrial purification. Various specific technologies are focused on for effective removal of dyes. In recent years, coagulation, chemical oxidation, photocatalytic degradation, membrane, and adsorption methods have been used extensively in dyes removal. Since many of these methods have disadvantages such as high investment, operating costs, excessive energy consumption, complex process stages and not being useful, more economical methods need to be designed to remove pollutants from water (Table 1). Among the methods used for purification processes, adsorption has been widely preferred recently because it is one of the most effective and applicable methods due to its high efficiency, easy operation and insensitivity to toxic substances compared to other methods [14–16]. In addition, the adsorption method is a process that provides effective results, especially in the removal of different types of dyestuff groups from wastewater. Correctly designed adsorption systems can provide high quality effluent. However, one of the

Table 1 Advantages and disadvantages of methods for dye removal

Methods	Advantages	Disadvantages
Ion exchange	No loss of adsorbent in regeneration	Not effective for all dyes
Photochemical	Zero sludge production	Formation of byproducts
Ozonation	Does not create mud Effluent volume remains same	High cost Short half-life (20 min)
Fentons reagent	Effective decolorization of both soluble and insoluble dyes	Sludge generation
Electrocoagulation	Effective removal of dyes	High cost Excess sludge production
Membrane filtration	Removal of all dye types	Expensive Concentrated sludge production
Chemical coagulation	Good color removal, economic	Sludge production
Adsorption	Excellent removal of wide varieties of dyes	Not economical (activated carbon)
Sonolysis	No sludge production	Dissolved oxygen requirement at high rate
Electrochemical destruction	Breakdown compounds are non-hazardous	High cost of electricity
Oxidation processes	Ease of application	Sludge formation at the end of the treatment process

biggest disadvantages of this method is the process cost. This cost is largely caused by the supply of adsorbent material.

It is of great importance to investigate cheap and easily available alternative adsorbents to reduce the purification cost of the adsorption method. Recycling has benefits such as protecting our natural resources, saving energy, contributing to the economy, and reducing the amount of waste. Recycling or recycling is the process of recycling waste that can be reused by turning it into a secondary raw material through various physical and/or chemical processes. Today, to prevent the harm to the environment and human health, solid waste types are collected and transported, as well as evaluation methods such as reuse, recovery and recycling.

Non-commercial low-cost adsorbents are generally used in leaves, fiber, fruit and vegetable peels, seeds, etc. Agricultural solid wastes and industrial by-products such as sawdust and tree barks are used as adsorbents due to some of their physicochemical properties [9, 14, 17, 18]. For example, sawdust, a by-product of the wood industry, is used as solid fuel or packaging material, and its cost is negligible [19]. Cellulose (40–50%), hemicellulose (20–40%) and lignin (20–30%) represent the major plant components [2]. Since sawdust contains organic compounds such as lignin, hemicellulose, and cellulose in its structure, it has been used in the adsorption of dyes, metals and other pollutants [20]. Khera et al. investigated the adsorption behavior of Cu, Ni, and Zn ions in single-metal system (SMS), bi-metal system (BMS), and tri-metal system (TMS) using *Archontophoenix alexandrae* as adsorbent. Generally, large amounts of waste emerge from the leaves and leaf sheaths of the *Archontophoenix alexandrae* plant. The plant contains a significant amount of fiber with a low ash content. In this study, the evaluation of plant wastes was investigated. The adsorption order in TMS was determined as $\text{Cu(II)} > \text{Zn(II)} > \text{Ni(II)}$. It is concluded that it is the specific properties of the binding site and solution chemistry that define the priority for adsorbents [21]. Kuncoro et al. presented an easy method of obtaining adsorbents from bagasse-bentonite mixture using bagasse waste and evaluated it from an environmental and solid waste management perspective. The prepared adsorbent was applied to remove Pb(II) from aqueous solution. The data obtained showed that it is a promising technique for the treatment of Pb-containing wastewater [22]. Kuncoro et al. in another study, they prepared an adsorbent from algal waste-bentonite mixture using algae waste and applied it to remove Pb(II) from aqueous solution. FTIR test results showed that there was a shift in the wave numbers on the Pb-loaded adsorbent; thus, they proved that there was an interaction between the adsorbent and Pb. From their results, they reported that the adsorption of Pb(II) with adsorbent prepared from algal waste-bentonite mixture is a promising technique for the treatment of Pb-containing wastewater [23]. Akkaya and Güzel found in their study that parsley stalks, cucumber peels, and watermelon seed hulls which are domestic wastes, can be used as biosorbents in their natural state as low-cost adsorbents in the removal of cationic dyes such as MB from aqueous solution [24]. Belala et al. in the removal of MB from aqueous solution of date stones and palm-trees waste [25], Mekuria et al. investigated the performances of barley bran and midrib leaf of *Ensete ventricosum* plant for the removal of MB from synthetic solutions by adsorption [26]. Grape leaves waste [27], sugarcane

bagasse and straw [28], turmeric leaves [29], areca leaves [29], banana stalk waste [30], pumpkin seed shells [31], banana stalks [32], ginkgo biloba [33] etc. vegetable wastes such as have been used in adsorption studies because they are low-cost or even cost-free and are abundant in nature.

Olive oil obtained from olives and olive have been important nutrients for humans for centuries. Olive leaf is a by-product of the olive tree that naturally contains many bioactive components with functional value. It is mostly released during pruning, harvesting and production activities of the olive tree and is very rich in polyphenolic compounds. When the olive is harvested from the tree, the leaves and branches mixed into the product are only 5% of the total product. In addition, because of pruning olive trees, approximately 25 kg of leaves and branches come out of one tree. During the processing of 1 ton of olives, 50–100 kg of olive leaf waste is generated. Since it has high cellulose, its value is low. Olive leaf is used in many areas as cosmetics, pharmaceutical industry, alternative medicine, and health support products with its versatile biological activities such as antioxidant, antithrombotic, anti-inflammatory, hypocholesterolemic, antimicrobial and antiviral due to the rich polyphenolic compounds it contains, especially oleuropein [34].

On the other hand, walnut has been included in the group of priority plants and classified as a strategic species for human nutrition by the United Nations Food and Agriculture Organization (FAO) due to its high nutritional value and rich in bioactive compounds. Walnut tree (*J. regia* L.) belongs to the Juglandaceae family and is widely grown worldwide (especially in Southeastern Europe, East Asia and North America) [35, 36]. It is stated that parts of the walnut tree such as green bark, leaf, brown bark, bark, root, branch, and shoot are also potential bioactive compounds [36]. As with olive leaves, 375 kg of leaf waste from walnut trees in one hectare area [37], it can be estimated that there are approximately 500 thousand tons of walnut leaves in 1.3 million hA. Since the walnut tree is a deciduous plant, it is understood that over 500 thousand tons of waste can be produced every year. As can be seen from these estimated data, olive leaves and walnut leaves create serious waste. These valuable agricultural wastes: considering their bioactive, chemical, and pharmacological properties, it is a sad situation to see that tons of food ingredients/raw material resources are thrown away without being evaluated or end up in nature every year. However, these resources, which are very valuable in terms of their chemical components and bioactive properties, are potentially raw materials.

Biopolymers are produced in nature by living organisms and plants, participate in the natural biological cycle, and eventually degrade in nature and rejoin the system. Chitin is the second most abundant biopolymer in the world after cellulose and has high potential for use in various fields. It is the main component of shellfish (such as crab, shrimp, oyster etc.). It is also found in insect shells and in the structure of the cell walls of fungi. Although there are many derivatives of chitin, the most important among them is chitosan, which is produced because of deacetylation of chitin [38]. Among the wastes of aquaculture enterprises, there are millions of tons of unused shellfish waste. The evaluation of these wastes is a very important issue both for the seafood industry and for public health. For these reasons, studies on chitosan gain value in preventing environmental pollution and waste utilization. Among the materials used to produce composites for separation processes, chitosan is one of

the most studied materials due to its hydrophilicity, very good forming ability, easy modification, and chemical stability [39–41].

Chitosan has a total of three reactive groups: primary (C-6) and secondary (C-3) hydroxyl groups and amine (C-2) group in each repeating unit. These reactive groups can easily undergo chemical modification and change the solubility as well as the mechanical and physical properties of chitosan. Chitosan must have a degree of deacetylation of 80–85% for good solubility [42]. In an acidic environment, the NH_2 group exists as $-\text{NH}_3^+$ and interacts electrostatically with the anionic groups in the environment. It exhibits cationic polyelectrolyte behavior in the protonated state, forming viscous solutions and interacting with oppositely charged molecules and surfaces. At low pH, amine groups are protonated and show polycationic properties, so chitosan in solution carries a positive charge in its structure. In this case, it can be easily dissolved in some solutions (formic, acetic, propionic, oxalic, malonic, succinic, adipic, lactic, pyruvic, malic, tartaric, and citric acid) in an environment defined as low pH, that is, $\text{pH} < 6.5$. Chitosan dissolves in acetic acid solution as chitosonium acetate because of the transformation of the free $-\text{NH}_2$ groups in its structure into the $-\text{NH}_3^+ -\text{OOCCH}_3$ structure. During the dissolution of chitosan in acetic acid, acetic acid does not affect *N*-acetyl ($-\text{NH}-\text{CO}-\text{CH}_3$) groups, but only reacts with $-\text{NH}_2$ groups.

In the cross-linking reaction of chitosan, the cross-linker is important for adsorption performance. Because this determines which functional groups of chitosan are consumed, formed, and incorporated. With this technique, the functional structures of chitosan are bonded to other functional groups with cross-linking agents to increase its adsorption capacity and resistance to environmental effects. Amino groups of chitosan are more active than hydroxyl groups not only in the adsorption process but also in cross-linking reactions. Supplementary Fig. 1. shows an example of chitosan cross-linked with glutaraldehyde. For example, Demarchi et al. synthesized a cross-linked-Fe(III) composite with glutaraldehyde and its performance in dye removal from aqueous media was examined [43]. As a result of the literature research, the suitable crosslinker for chitosan was chosen as glutaraldehyde.

Undoubtedly, the most important feature of magnetic nanoparticles in terms of water treatment is that they can be easily separated from aqueous streams using an external magnetic field. This easy separation of the adsorbent from the aqueous stream without requiring centrifugation or filtering processes makes the process more economical as it reduces the expenses required for separation processes. The biocomposites synthesized in the study were given magnetic properties, allowing them to be easily separated from aqueous environments.

It is important that some plant wastes that are out of use are transformed into new raw materials for reuse by going through various processes. Considering the properties of chitosan, walnut leaf/olive leaf and magnetic nanoparticles, and since there is no report on the synthesis of this composite in the literature, this research aimed to design a beaded polymeric composite derived from chitosan, walnut leaf/olive leaf and magnetic nanoparticles. In this direction, walnut, and olive tree leaves, which are waste materials, were immobilized with chitosan and made magnetic with nFe_3O_4 , and the adsorption of MB dye onto biocomposite adsorbents was examined in a batch system. Thus, high-capacity adsorbents have been prepared by both

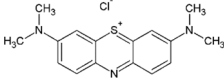
utilizing unused and abundant biowastes in nature and creating composites containing a wide spectrum of surface functional groups. On the other hand, instead of costly/intrusive processes such as filtering and centrifugation to remove adsorbents from the aqueous medium, the removal step has been facilitated by bringing the adsorbent into magnetic form. The novelty of this strategy is based on the combination of vegetable wastes, which are quite abundant as waste in the environment, with magnetic particles and chitosan for the production of bioadsorbents to improve its adsorptive property for the removal of a cationic dye such as methylene blue. Its main advantages can be seen as follows: (i) the easy separation offered by magnetic particles and (ii) the use of properties of chitosan already known in the scientific community. Therefore, this article presents a new interdisciplinary horizon at the frontier of biopolymers, plant biochemistry, water purification industry and environmental protection. The synthesis of new magnetic biocomposite adsorbents cross-linked with glutaraldehyde, prepared with superior chitosan and wood waste, and their use in the removal of MB dye was carried out for the first time in this study. For this purpose, the effects of ambient pH, adsorbent dose, temperature, contact time and initial MB concentration parameters on MB adsorption in the batch system were examined. Moreover, this article also presented different thermodynamic parameters such as Gibbs free energy change (ΔG°), enthalpy change (ΔH°) and entropy change (ΔS°). For this purpose, it is aimed that adsorbents for MB removal from aqueous solutions can be produced with biocomposites prepared from chitosan and plant wastes.

Materials and methods

Materials

Chit flakes (degree of deacetylation, DD = 75–85%), iron(II, III) oxide (Fe_3O_4) nanopowder and glutaraldehyde (25% in H_2O) (CAS No.: 111-30-8) were purchased from Sigma-Aldrich. NaOH, HCl, and acetic acid were purchased from Merck Company. MB was purchased from Acros Organics (molecular weight: $319.85 \text{ g mol}^{-1}$, molecular formula: $\text{C}_{16}\text{H}_{18}\text{ClN}_3\text{S}\cdot x\text{H}_2\text{O}$) (Table 2). All related chemicals used in the experiments were of analytical grade. In preparing the composite adsorbent, thermostated shaker of the GFL 3033 model, IKAMAG-RO15 model mechanical stirrer, and a pH meter (Orion 900S2) with glass electrode were used. Biowastes were ground into powder form using a blender (Isolab Laborgerate GmbH). In the characterization of the synthesized m-WCH and m-OCH, the size and morphology of the structure were determined by SEM (Nova NanoSEM 200, FEI Company) and the possible functional groups in the structures were determined by the FTIR analysis method (Bruker VERTEX 70 FTIR spectrometer). X-ray diffractometry (XRD) was used to determine the crystalline structures of m-WCH and m-OCH. XRD analysis was performed at Konya Technical University, Central Research Laboratories, in GNR EUROPE 600 XRD model device, $\text{CuK}\alpha$ radiation, running conditions of 40 mA, 40 kV with 2θ ranging from 10 to 90° at scan speed 0.005° , and time/scan

Table 2 Physicochemical properties of MB

M (g mol ⁻¹)	319.85
Molecular formula	C ₁₆ H ₁₈ ClN ₃ S · xH ₂ O
Structural formula	
λ_{max} (nm)	664
Physical form	Crystalline powder with metal luster
Color	Green powder
Solubility	Solubility in water: soluble. Other solubilities: soluble in alcohol and chloroform, insoluble in ether
Storage temperature	Room temperature

0.1 s. UV–visible spectrophotometer (Shimadzu UV-1700) was used to determine MB (λ_{max} : 664 nm).

Biowaste powder preparation

In this study, walnut tree (WL) and olive tree leaves (OL) were used as wood waste. WL and OL were first washed to remove dust and dirt and rinsed with distilled water. Then it was dried in the oven at 60 °C. WL and OL were pulverized with the help of a blender and washed first with 0.1 M HCl, then with pure water and dried. The dried leaves were sieved by sieve analysis to a particle size below 125 μm (Fig. 1). The prepared leaf powders were used in the composite synthesis in their natural form without any modification process.

Preparation of m-WCH and m-OCH Beads

In the first step of the synthesis of composite beads, chitosan (2% w/v) was added to acetic acid solution (150 mL, 2% v/v) and mixed for 24 h until gelation. After the chitosan was completely dissolved, WL/OL (1.5 g) and nano Fe₃O₄ (1 g) were added and the final mixture was left to mix in a mechanical mixer for 3 h to obtain the nano Fe₃O₄-WL/OL-CHT biocomposite. Composite beads were obtained by dropping the prepared mixture into sodium hydroxide solution (600 mL

Fig. 1 WL powder (a) OL powder (b)

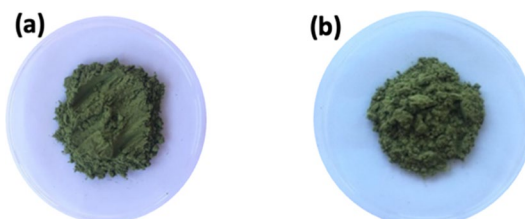




Fig. 2 Schematic diagram of preparation of m-WCH and m-OCH and adsorption of MB

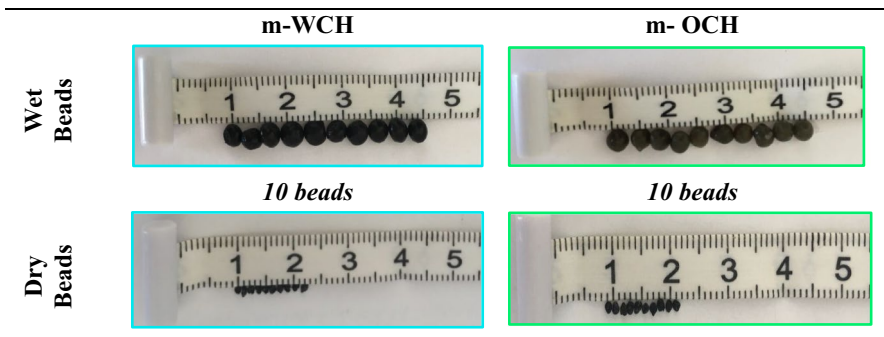


Fig. 3 Photographic images of wet and dried m-WCH and m-OCH hydrogel beads

methanol, 400 mL water and NaOH (120 g)) dropwise using a burette and kept in a this solution bath overnight. The beads were then filtered and washed until the medium was neutral to remove excess acetic acid. For the ionic cross-linking reaction of the beads with glutaraldehyde, they were mixed at 60–70 °C for 30 min. At the end of the reaction, the composite beads were filtered and washed several times with deionized water, dried at 60 °C and stored until use. Figure 2. shows the process of immobilization of WL/OL with chitosan. The photographs of wet, and dried beads are shown in Fig. 3.

Moisture content

The moisture content was determined WL, OL and immediately after m-WCH and m-OCH composite beads making. Material was dried at 103 °C, cooled in a desiccator, and weighed. The process was repeated until fixed weighing. The amount of moisture was found by weight loss, calculated as the weight percentage (ASTM D 2016-74) [44]. The moisture content (MC, %) was calculated according to the Eq. (1):

$$MC(\%) = \frac{m_o - m_d}{m_o} \times 100 \quad (1)$$

where m_o and m_d are the mass of the adsorbent before and after drying, respectively. In order to obtain an average value, the experiment was repeated three times for each sample.

Adsorption experiments

MB removal was carried out in a batch system with m-WCH and m-OCH composites. Stock solution was prepared with MB and the concentrations to be used in the experiments were prepared by diluting from the stock solution. In the experimental system, solution pH, initial MB concentration, contact time, amount of adsorbent and temperature parameters were examined, and the best removal conditions were determined. Solution pH adjustments were made with 0.1 M NaOH and 0.1 M HCl. The concentration of MB remaining unadsorbed in the samples taken from the system was determined spectrophotometrically by reading the absorbance on a spectrophotometer (UV-1700, Shimadzu) at 664 nm. In the adsorption of MB molecules with m-WCH and m-OCH composites, the % adsorption and q_e (mg g⁻¹) were calculated with the equations given below (Eqs. 2, 3);

$$q_e = (C_o - C_e)V/m \quad (2)$$

$$\% \text{ Adsorpsiyon} = C_o - C_e/C_o \times 100 \quad (3)$$

Here, C_o is the initial concentration (mg L⁻¹), C_e is the concentration of the substance remaining unadsorbed at equilibrium (mg L⁻¹), V is the solution volume (L) and m is the adsorbent mass (g).

Selectivity study

The selective adsorption of the m-WCH and m-OCH was studied for different mixtures of methyl orange and MB. Competitive adsorption studies was conducted by adding the interfering dye (MO) with different concentration between 2 and 16 mg/L in to the 25 mL of MB ion sample solution 14 mg/L [45]. The mixing solution was

stirred on a shaker for 120 min at pH 6. Distribution, selectivity coefficient and relative selectivity coefficient were calculated using Eqs. 4, 5 and 6 below [45, 46]:

$$K_d = \frac{C_i - C_f}{C_f} \left(\frac{V}{m} \right) \quad (4)$$

where K_d , C_i , C_f , V and m are distribution coefficient, initial concentration (mg/g), final concentration (mg/g), volume of solution (L), and mass of adsorbent (g), respectively. Selectivity coefficient for binding of molecules target in present of a competitor ion can be used the Eq. (5) [47]:

$$k = \frac{K_d(\text{target})}{K_d(\text{interferent})} \quad (5)$$

where k is coefficient of selectivity. In order to evaluate an imprinting effect, a relative selectivity coefficient (k') was defined as follows Eq. (6) [46]:

$$k' = \frac{k(\text{imprinted})}{k(\text{non imprinted})} \quad (6)$$

Determination of pH_{PZC}

The PZC determination was performed according to the procedure reported in Budiana et., al (2021) and Neolaka et., al (2020) [45, 46]. 9 (nine) vessels where contain with 0.01 mol/L NaCl 10 mL were added with 0.1 mol/L NaOH or 0.1 mol/L HCl to conditioning the initial of pH from 1 to 9. Then, 30 mg of m-WCH or m-OCH were added and shaken for 48 h at room temperature (28 °C) on shaker at 200 rpm. After this period, final pH was measure with pH meter. The pH data obtained are then curved toward the initial pH. The point of intersection between the final pH and the initial pH is the pH_{PZC} value [45].

Mathematical description of adsorption system

Isotherm modeling

The adsorption isotherm is a graphical representation that expresses the relationship between the amount sorbed by a unit weight of a sorbent and the amount of contaminant remaining in a solution medium at equilibrium. Therefore, the equilibrium process of the solute between the liquid and solid phases can be explained by isotherm curves [48]. In this study, to define the adsorption system, the experimentally obtained data were applied to the Langmuir, Freundlich, Scatchard, Dubinin–Radushkevich and Temkin isotherm models and the parameters of each isotherm were determined.

In the Langmuir isotherm model, it is assumed that adsorption occurs on a single layer and the surface is homogeneous. The linear formula is defined as follows (Eq. 7) [49]:

$$C_e/q_e = 1/K_L q_m + C_e/q_m \tag{7}$$

Constants given in the Langmuir isotherm; q_e is defined as the amount of pollutant adsorbed on the unit adsorbent (mg g^{-1}), C_e is the concentration of pollutant without being adsorbed in the liquid (mg L^{-1}), q_m is the Langmuir maximum adsorption capacity (mg g^{-1}), K_L is the constant depending on the adsorption energy (L mg^{-1}). The separation factor, R_L , can be calculated using Eq. 8.

$$R_L = 1 / (1 + K_L C_o) \tag{8}$$

The Freundlich adsorption isotherm model is applied in adsorption processes on heterogeneous surfaces. The Freundlich adsorption isotherm model is defined by Eq. 9 [50];

$$\log q_e = \log K_F + 1/n \log C_e \tag{9}$$

K_F is defined as the adsorption constant, n as the degree of adsorption, q_e as the amount of substance adsorbed on the unit adsorbent (mg g^{-1}), C_e as the concentration of pollutants remaining unadsorbed in the liquid (mg L^{-1}).

Scatchard analysis is a method that can give more specific results than Langmuir and Freundlich isotherms in terms of examining the characteristics and various parameters of the adsorbed substance. When a significant deviation from linearity is observed in the Scatchard plot, it is expected that it approaches the Freundlich isotherm and moves away from the Langmuir isotherm, considering that physical adsorption occurs instead of chemical adsorption. For adsorption from solution, the Scatchard model expressed as Eq. (10) [15].

$$q_e/C_e = Q_s K_s - q_e K_s \tag{10}$$

Here q_e gives the maximum capacity, K_s gives the dissociation constant, and C_e gives the concentration of pollutants remaining unadsorbed in the liquid.

The Temkin isotherm model assumes that the adsorption heat of all molecules in the layer decreases linearly as a result of the surface being covered with the pollutant and is defined by Eq. 11 below [50];

$$q_e = B \ln K_t + B \ln C_e \tag{11}$$

B is a constant related to the heat of sorption (J mol^{-1}) and K_t is defined as the equilibration isotherm equilibrium binding constant (L mg^{-1}).

The D–R isotherm model provides information about the physical or chemical nature of the interaction between the pollutant and the sorbent material on a heterogeneous sorbent surface. The equation of this model, which is also used to determine the average sorption energy (E), is given below (Eq. 12).

$$\ln q_e = \ln q_m - \beta \epsilon^2 \tag{12}$$

Here; β : D–R constant related to the average free energy ($\text{mol}^2 \text{J}^{-1}$), q_e : Adsorption capacity at equilibrium (mol g^{-1}), q_m : Theoretical saturation capacity of the sorbent (mol g^{-1}), ϵ : It is obtained by the equation Polanyi potential

(mol kJ⁻¹). The fact that the E value is between 8 and 16 kJ mol⁻¹ indicates that chemical ion exchange is involved in the process, and that this value is less than 8 kJ mol⁻¹ indicates that the process occurs by physical sorption [51].

Kinetic models

While adsorption kinetic studies provide information about the possible sorption mechanism and different transition states leading to the formation of the pollutant-adsorbent complex, they also help to develop appropriate mathematical models to describe possible interactions. In general, adsorption onto porous solids is assumed to occur in several steps. The first step is external diffusion, the second step is due to the transport of the solute across the boundary layer, the third step is the uptake of the pollutant into the pores and active sites of the adsorbent, and the fourth step involves adsorption and desorption. Pseudo-first-order, pseudo-second-order kinetic models, Elovich kinetics model, and intraparticle diffusion model are frequently used in the kinetic evaluation of adsorption based on the adsorption rate of adsorbents.

The equation of the pseudo-first-order kinetic model (Eq. 13) is a model that is based on the concentration of the solution, the adsorption capacity of the adsorbent and defines the adsorption rate. This equation has become one of the most used equations for kinetic modeling in adsorption:

$$\ln(q_e - q_t) = \ln q_e - k_1 t \quad (13)$$

Here; t : time (min), k_1 : Lagergren pseudo-first-order rate constant (min⁻¹), q_e : Adsorption capacity at equilibrium (mg g⁻¹), q_t : The amount of substance biosorbed at any time (mg g⁻¹) [52].

The pseudo-second-order kinetic model describes chemical adsorption involving the sharing of electrons or valence forces through chemical exchange between the adsorbent and the adsorbent. This model can be expressed by the following Eq. (14).

$$\frac{1}{q_t} = \frac{1}{k_2 q_e^2} + \frac{1}{q_e t} \quad (14)$$

Here; k_2 : Pseudo-second-order rate constant (g mg⁻¹ min⁻¹), q_t : Adsorption capacity at time t (mg g⁻¹) q_e : Maximum Adsorption capacity (mg g⁻¹) [53].

Elovich model was expressed using the following Eq. (15):

$$q_t = \frac{\ln \alpha \beta}{\beta} + \frac{\ln t}{\beta} \quad (15)$$

Here; t : Adsorption time (min), q_t : Adsorption capacity at certain time (mg g⁻¹), α : Initial adsorption rate constant of Elovich model (mg g⁻¹ min⁻¹) and β : the desorption constant associated with the surface area coverage, and chemisorption activation energy (g mg⁻¹) [54]. The data collected from q_t and $\ln t$ were plotted to obtain the value of β , α , and R^2 .

Weber and Morris formulate the intra-particle diffusion model to locate the migration of adsorbates from the surface of adsorbent into its internal pores because of stirring process as follows (Eq. 16):

$$q_t = k_{id}t^{0.5} + C \quad (16)$$

Here: k_{id} : the constant of intra-particle diffusion ($\text{mg g}^{-1} \text{min}^{-0.5}$), C : the intercept (mg g^{-1}). The value of k_{id} is obtained by plotting q_t versus $t^{0.5}$. To attest that the adsorption mechanism obeys this model, a linear relationship is obtained when q_t versus $t^{1/2}$ is plotted and the values K_{id} and C can be found through linear fitting analysis [55]. The C has a characteristic relationship with the boundary layer thus the higher the value of C , the larger the effect of the boundary layer ensues [46].

Results and discussion

Characterization of composites

In the characterization of the synthesized m-WCH and m-OCH, the size and morphology of the structure were determined by SEM, EDX, mapping and possible functional groups in the structure were determined by FTIR analysis. The crystal structure of the synthesized composite was determined by XRD analysis.

SEM/EDX and specific surface area analysis

During the adsorption process, the change in the surface of m-WCH and m-OCH was examined by scanning electron microscopy (SEM). Scanning electron microscope is a type of electron microscope that obtains images by scanning the sample surface with a focused beam of electrons. Electrons interact with the atoms in the sample and produce different signals containing information about the sample surface. These signals are collected by the relevant detectors and images are obtained [56]. Surface images of m-WCH and m-OCH recorded at different magnifications before the adsorption process are given in Supplementary Fig. 2a, c. As seen in the figure, there are rough structures, cavities, and pores on the surfaces of m-WCH and m-OCH. Such surfaces represent structural suitability that can be considered important for the binding of MB molecules to different parts of the material. As seen in SEM images the surfaces of m-WCH and m-OCH are different from each other before and after adsorption. It is clearly seen that after adsorption, the gaps, cavities and pores on the surfaces of the composite adsorbents decrease and turn into a structure with a less porous surface (Supplementary Fig. 2b, d). This confirms that these differences in the structure of the adsorbents adhere to the MB molecules on the composite surface.

Elemental mapping and multipoint analysis via EDX were performed to confirm the compositions of the surfaces and observed structures. MB particles were found on the surfaces of the adsorbents after MB adsorption. EDX analysis results revealing the elemental composition of m-WCH and m-OCH adsorbents

before and after MB adsorption are given in Supplementary Fig. 3–6. According to the data obtained from EDX spectra; Elemental composition of m-WCH composite (by weight); 63.14% O, 25.40% C, 2.15% Fe, 3.03% S and 6.26% N, and its elemental composition (by weight) after MB adsorption; 59.13% of it was determined as O, 25.97% as C, 2.31% as Fe, 3.23% as S and 9.36% as N. On the other hand, according to the data obtained from EDX spectra; Elemental composition of m-OCH composite (by weight); 54.75% O, 28.32% C, 2.45% Fe, 2.99% S and 11.49% N, and its elemental composition (by weight) after MB adsorption; 59.25% of it was determined as O, 26.16% as C, 1.15% as Fe, 3.50% as S and 9.94% as N. Fe amounts confirm that it contains Fe₃O₄ nanoparticles in m-WCH and m-OCH structures. A greater amount of sulfur was present on the surface after MB adsorption compared to before adsorption, indicating MB adsorption. This indicates the preferential adsorption of MB to the surface of the composite, possibly due to a greater number of active sites than m-WCH and m-OCH or limited diffusion of adsorbates through the pores [57].

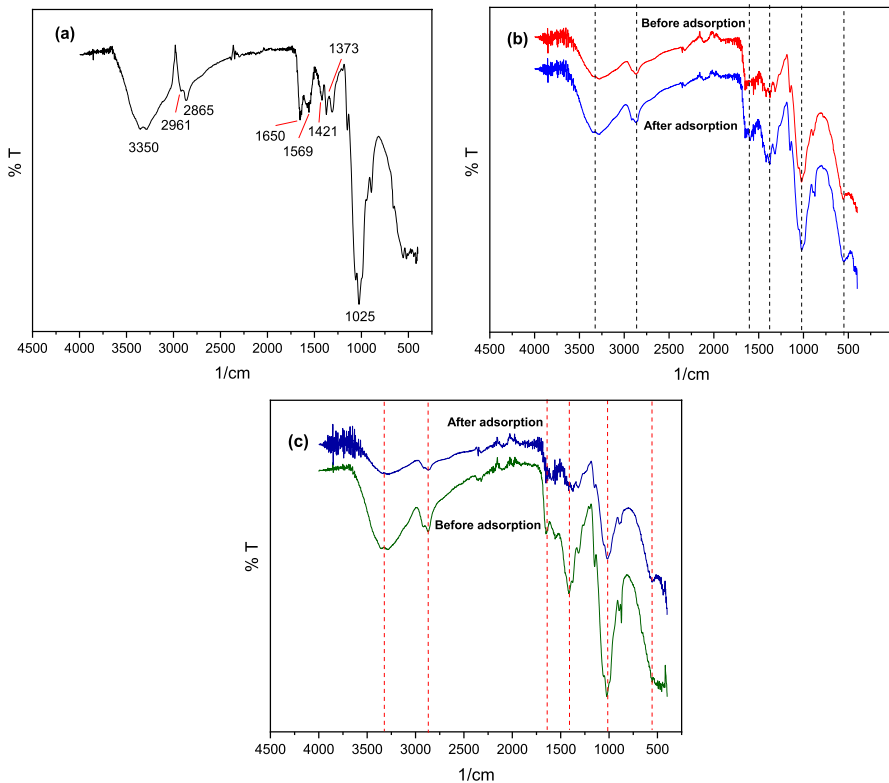


Fig. 4 FTIR diagram of **a** Chitosan, **b** m-WCH before and after MB adsorption, **c** m-WCH before and after MB adsorption

FT-IR analysis

The FTIR spectra of Chitosan, m-WCH before and after MB adsorption, m-OCH before and after MB adsorption are given in Fig. 4a, b, and c, respectively. When the spectrum of chitosan is examined, a strong band is seen in the 3240–3450 cm^{-1} region. This peak arises from the coincidence of O–H stresses and N–H stresses in the structure of chitosan [49]. The absorption bands around 2961 cm^{-1} and 2865 cm^{-1} are C–H symmetric and asymmetric stretching vibrations, respectively, belonging to aliphatic CH_2 groups [58]. The tensions of the C=O bonds in the acetyl units of chitosan are observed around 1650 cm^{-1} , and the peak resulting from N–H tensions is observed at 1569 cm^{-1} . The CH–OH bending vibration and CH_2 –OH symmetric deformation vibrations in the structure were confirmed by the presence of bands around 1421 cm^{-1} and 1373 cm^{-1} , respectively [59]. Another important characteristic peak of chitosan is the peak observed at 1025 cm^{-1} , which is known to belong to C–O–C stretches.

To determine the functional groups, present on the surface of m-WCH and m-OCH adsorbents and the functional groups involved in MB adsorption, FTIR spectra of the adsorbents before and after adsorption were taken (Fig. 4b, c). In the FTIR spectra of m-WCH and m-OCH taken before adsorption; the peaks observed at 3300, 3315 cm^{-1} indicate the presence of –OH and N–H groups on the surface. Beads cross-linked with glutaraldehyde show an increase in the intensity of the peaks at 2882 and 2871 cm^{-1} [58]. This represents the existence of symmetric stretching of C–H₂ and C–H. The explanation for this is that the glutaraldehyde molecule can cause an increase in the cross-linked chain by contributing to the reaction. The peaks at 1630 and 1648 cm^{-1} in m-WCH and m-OCH composite adsorbents, respectively, belong to amide I and II groups and are characteristic peaks of biowaste structures and chitosan. This peak value in the compound indicates that plant wastes and chitosan were successfully combined. In the structure of composite adsorbents, the peak corresponding to the NH-bonding vibrations in the amine group of chitosan is observed at 1575 cm^{-1} . The bands occurring in the region between 1500–1200 cm^{-1} may be related to NH, O–C–H, C–C–H and C–O–H bendings [49, 60, 61]. The peaks occurring around 1020 cm^{-1} and 1025 cm^{-1} may result from C–O stretching of lactone or carboxyl groups. The sharp peaks at 565 and 545 cm^{-1} represent the Fe–O absorption bands of Fe_3O_4 [44].

When the spectra of m-WCH and m-OCH composites before and after MB adsorption are compared, since the changes in peak frequencies correspond to changes in the energy of the functional group, changes such as shifting or disappearing after adsorption are an indication that those peaks play a role in adsorption. These results prove the adsorption of MB to the functional groups of the above-mentioned m-WCH and m-OCH composites. For example, after MB adsorption of the m-WCH composite, the peak detected at 3300 cm^{-1} in the FTIR spectrum shifted to 3274 cm^{-1} , the peak at 2882 cm^{-1} shifted to 2871 cm^{-1} , and the peak at 1591 cm^{-1} shifted to 1557 cm^{-1} . It was observed that the peak at 1386 cm^{-1} shifted to 1374 cm^{-1} , the peak at 1011 cm^{-1} shifted to 1031 cm^{-1} , and the peak at 565 cm^{-1} shifted to 550 cm^{-1} . After MB adsorption of the m-OCH composite, the peak detected at 3315 cm^{-1} in the FTIR spectrum shifted to 3289 cm^{-1} , the peak at

2871 cm^{-1} shifted to 2862 cm^{-1} , and the peak at 1648 cm^{-1} shifted to 1656 cm^{-1} . It was observed that the peak at 1405 cm^{-1} shifted to 1375 cm^{-1} , the peak at 1024 cm^{-1} shifted to 1015 cm^{-1} , and the peak at 545 cm^{-1} shifted to 562 cm^{-1} . In addition, after MB adsorption, it is seen that the band around 3300 and 3315 cm^{-1} for m-WCH and m-OCH, respectively, narrows in the spectrum. The reason for this sharp decrease is thought to be due to ionic interactions between the $-\text{OH}$ groups in the structure and the dyestuffs. The shift of the bands may indicate that these functional groups interact with MB molecules.

XRD analysis

XRD patterns of chitosan (Supplementary Fig. 7a), nano Fe_3O_4 (Supplementary Fig. 7b), m-WCH composite (Supplementary Fig. 7c) and m-OCH composite (Supplementary Fig. 7d) are shown. Broad peaks indicate very fine and small crystallite sizes, while sharp peaks indicate a polycrystalline structure [62, 63]. Supplementary Fig. 7c,d shows the XRD patterns of m-WCH and m-OCH composites. WL and OL consist mainly of crystalline cellulose, non-crystalline hemicellulose and lignin [64]. The diffraction peaks for the crystalline form of cellulose I, which is attributed to most natural cellulose, are at $2\theta=16.11$ and 22.41 [65]. On the other hand, characteristic Fe_3O_4 peaks were clearly observed. These peaks were $2\theta=20.02^\circ$, 36.59° , 44.31° , 58.29° and 63.92° [66]. In this study, the chitosan XRD pattern shows $2\theta=20.80^\circ$. Karimi [67] reported that chitosan has the typical peak at $2\theta=19\text{--}20^\circ$. It confirms that nano- Fe_3O_4 and tree leaf combine with chitosan. The peak intensity decreases and the full width of the peak increases; This indicates the low crystallinity and small crystal size of Fe_3O_4 particles.

pH_{PZC} determination

The Point of Zero Charge (pH_{PZC}) is the condition that on the surface of adsorbent has a neutral charge. pH_{PZC} is an important parameter to assess the ease of analyte

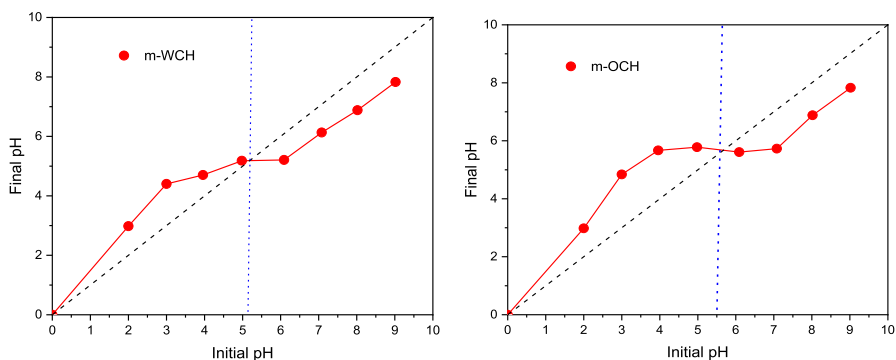


Fig. 5 pH_{pzc} for m-WCH and m-OCH

adsorption on the surface of the adsorbent [68]. The determination result of pH_{PZC} is shown in Fig. 5. Figure 5 shows that the PZC value for m-WCH and m-OCH are 5.20 and 5.50, respectively. At pH values lower than pH_{PZC} , the adsorbent has a positive surface charge that promotes the adsorption of negatively charged compounds. On the other hand, when the pH is greater than pH_{PZC} , the adsorbent has a negative surface charge, which promotes positively charged compound adsorption. Therefore, knowing this value helps in deciding which pH to work at in adsorption studies. It can therefore be concluded that the adsorption of MB dye by m-WCH and m-OCH should be favored in media with a pH greater than 5.5.

Moisture content

Samples were analyzed for moisture content and listed in Table 3. The moisture contents of WL powder and OL powder were found to be 5.5 and 6.9, respectively. It was observed that the moisture content of OL powder was slightly higher than that of WL powder. On the other hand, for m-WCH and m-OCH prepared using WL and OL, most of the water was removed from the beads and the moisture content was low compared to fresh and after drying at room temperature (Table 3). Water in a sample or product is either free or bound to the matrix by different forces. In air-drying process, the application of air removed water from beads by the process of evaporation, but some water was still bound to the matrix by various forces.

Adsorption properties of m-WCH and m-OCH beads

Initial MB concentration effect

The initial dye concentration provides a significant driving force for the dye molecules to overcome any mass transfer resistance between the aqueous and bulk phases. Therefore, the change of initial MB concentration is an important factor that should be investigated in all adsorption studies. In order to examine the effect of the initial MB concentration on the adsorption system, the MB concentration range was chosen as 10–250 ppm. Experiments were carried out at 6 gL^{-1} adsorbent dosage and pH 6. MB solutions of m-WCH and m-OCH adsorbents were shaken separately at 298 K for 120 min with the help of a shaker. After shaking, the concentration

Table 3 Moisture content of WL, OL, m-WCH fresh/dried beads and m-OCH fresh/dried beads

Material	Moisture content (%)
WL powder	5.5
OL powder	6.9
m-WCH fresh beads	92.2
m-WCH dried beads	3.2
m-OCH fresh beads	90.6
m-OCH dried beads	5.1

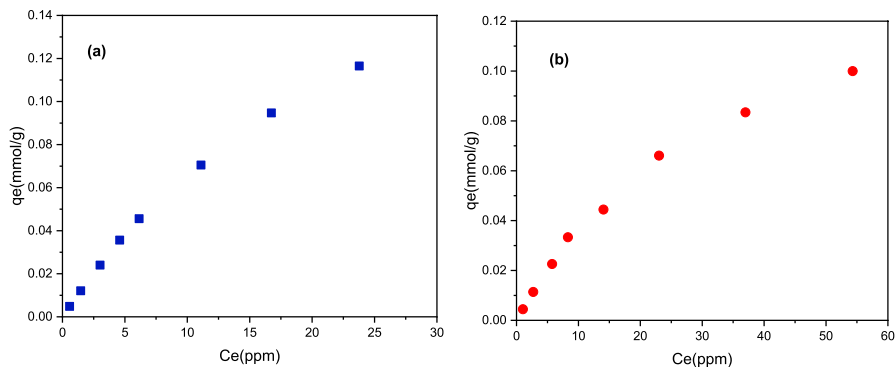


Fig. 6 Effect of initial concentration on the removal of MB onto m-WCH (a) and m-OCH (b)

of MB remaining unadsorbed was determined by UV–Vis. In Fig. 6, the effect of the MB concentration removed from the aqueous solution on the initial concentration can be seen. As the MB concentration increases, the driving force increases and the adsorbed MB concentration increases. For both composites, as the concentration of the MB solution increases, MB adsorption initially increases rapidly, then slows down and remains constant after a certain period of time (Fig. 6). This is a possible result of the saturation of the active sites of MB and m-WCH and m-OCH. It is thought to be due to the fact that the adsorbent has a limited number of active sites that become saturated at a certain dye concentration [61]. Although the driving force required above the mass transfer resistance of the dye molecules to hold on to the solid surface increases with increasing concentration, considering that the adsorbent surface has a limited number of active centers for the adsorption of dye molecules, with increasing concentration, the dye molecules in the aqueous solution will increase this limited active center on the adsorbent surface. It should be taken into account that the possibility of contact with centers will decrease [69, 70]. Therefore, in more dilute dye solutions, the ratio of active centers to MB dye molecules in the solution will be higher, resulting in a higher dye removal percentage compared to concentrated dye solutions [71].

Adsorption isotherm

In order to investigate the equilibrium behavior of m-WCH and m-OCH; Freundlich, Langmuir, Dubinin–Radushkevich, Scatchard and Temkin isotherm models were used. Isotherm models explain the relationship between the surface properties of the substance used as an adsorbent, the amount of adsorbate remaining unadsorbed in the solution, and the amount of adsorbate adsorbed by the adsorbent. While the Langmuir isotherm model accepts that single-layer adsorption of MB molecules occurs on equally energetic adsorption sites on m-WCH and m-OCH, the Freundlich isotherm model accepts that adsorption occurs on multi-layered and non-equivalent adsorption sites. However, the Dubinin–Radushkevich isotherm model assumes that adsorption can occur on homogeneous and heterogeneous surfaces. The Temkin

Table 4 Adsorption isotherm constants of MB onto m-WCH and m-OCH

Model	Adsorbent	Parameters for dye			
		A_s	K_b	R^2	R_L
Langmuir	m-WCH	85.47	0.0327	0.996	0.234
	m-OCH	53.48	0.0273	0.993	0.268
		K_f	n	R^2	
Freundlich	m-WCH	2.788	1.164	0.993	
	m-OCH	1.66	1.271	0.984	
		$X_m \times 10^{-2}$	K	E	R^2
D–R	m-WCH	0.260	0.0062	8.98	0.999
	m-OCH	0.127	0.0061	9.05	0.995
		Q_s	K_s	R^2	
Scathard	m-WCH	86.35	0.0323	0.991	
	m-OCH	54.43	0.0267	0.970	
		B	K_t	R^2	
Temkin	m-WCH	9.63	1.098	0.891	
	m-OCH	7.91	0.645	0.922	

isotherm model accepts that the adsorption heats of all molecules decrease linearly with increasing surface coverage.

Adsorption equilibrium data of Langmuir, Freundlich, Scatchard, Temkin and Dubinin–Radushkevich models are given in Supplementary Fig. 8. The parameters calculated using the data obtained from these models are also given in Table 4. Adsorption constants obtained from the Freundlich model are also shown in Table 4. K_f and n values were calculated as 2.788 and 1.164, respectively, for m-WCH. K_f and n values were calculated as 1.66 and 1.271 for m-OCH, respectively. n values between 1 and 10 indicate that adsorption is good. A value of n greater than one indicates favorable adsorption conditions. Temkin isotherm was applied to determine the binding energies of adsorption processes. In adsorption processes, it refers to chemical adsorption as an electrostatic interaction [72]. Considering the correlation constants ($R^2=891$ (m-WCH) $R^2=922$ (m-OCH)), the experimental data showed a good adaptation to the Temkin isotherm. This high correlation coefficient has been shown that an important mechanism affecting the interaction between m-WCH and m-OCH with MB is the electrostatic interaction [73]. It was found that the Temkin constants were $K_t=1.096$ (m-WCH) and 0.645 (m-OCH) and $B_T=9.63$ (m-WCH) and 7.91 (m-OCH). The E value calculated from the D–R isotherm model was obtained as 8.98 and 9.05 for m-WCH and m-OCH, respectively. E values show that MB adsorption with m-WCH and m-OCH occurs chemically. When the Table 4. is examined, it is seen that the equilibrium data obtained from adsorption on m-WCH and m-OCH for MB adsorption is best compatible with the Langmuir isotherm model. The correlation values for the Langmuir isotherm model for the adsorption

of MB onto the synthesized m-WCH and m-OCH were found to be 0.996 and 0.993, respectively. Considering the best correlation value, it can be said that the adsorption process is more compatible with the Langmuir isotherm. It was observed that MB was directed to specific homogeneous regions on the adsorbent and adsorption took place in these regions. It can also be said that the adsorption process occurs in a single layer. This shows that each dye molecule has equal adsorption activation energy in adsorption to the adsorbent surface [61]. The Langmuir isotherm alone is not sufficient to explain the equilibrium state for homogeneous adsorption systems. The dimensionless separation factor R_L values for the adsorption of MB onto the adsorbent are given in Table 4. As can be seen, (R_L) values for all concentrations are between 0 and 1. R_L values between 0 and 1 indicate that the adsorption process is monolayer and more favorable [61]. The maximum monolayer adsorption capacity obtained from the Langmuir isotherm for m-WCH and m-OCH was found to be 85.47 mg g⁻¹ and 53.48 mg g⁻¹, respectively. The fit of this model also confirms the possible irreversibility and chemisorption of the process. Q_s and K_s constant values were calculated to determine the suitability of the Scatchard isotherm. In this isotherm, the maximum capacity for m-WCH and m-OCH was found to be 86.35 and 54.43 mg g⁻¹, respectively, and R^2 values were 0.991 and 0.970, respectively. These

Table 5 Comparison of adsorption capacities of different adsorbents for MB removal

Adsorbent	q_e (mg g ⁻¹)	References
Fe ₃ O ₄ /graphene/chitosan nanocomposite	94.16	[74]
Magnetite nanoparticles loaded fig leaves	61.72	[50]
Magnetite nanoparticles loaded Azolla	25	[50]
Potato leaves	52.6	[75]
Lemongrass leaves	43.16	[76]
<i>Ficus Palmata</i> leaves	6.8	[77]
<i>Ginkgo biloba</i> leaves	48.1	[33]
<i>Azadirachta indica</i> leaves	19.6	[78]
Rice husk	40.5	[79]
Walnut shell	36.631	[80]
Banana stalks	20.8	[32]
Orange peel	18.6	[81]
Ginger StrawWaste-derived porous carbons	62.54	[82]
Magnetized chitosan nanocomposite	76.34	[83]
Chitosan/organic rectorite-Fe ₃ O ₄ intercalated composite	24.69	[84]
Magnetic nanocomposites of cellulose	40.5	[85]
Magnetic activated carbon/chitosan	24.5	[86]
Apricot stones activated carbon	36.68	[87]
Chitosan/citric acid modified pistachio shell/halloysite nanotubes	111.14	[58]
Iron impregnated AC	30.61	[88]
m-WCH	85.47	This study
m-OCH	53.48	This study

values support the suitability of the Langmuir isotherm. In Scatchard analyzes, when the graph approaches linearity, it indicates that it is approaching the Langmuir isotherm. This indicates that the adsorption is closer to monolayer adsorption.

There are previous similar studies in the literature for the adsorption of MB molecules (Table 5). When compared to similar studies in the literature, the adsorption capacity found as a result of this study is seen to be better than some, but also lower than some. It was observed that the synthesized m-WCH and m-OCH composite had a usable potential in MB removal.

Effect of adsorbent dosage

Another parameter that plays an important role in adsorption processes is determining the most appropriate amount of adsorbent to be used. Because this determines the capacity of an adsorbent for a given initial MB concentration. To determine the effect of the amount of adsorbent on MB adsorption, studies were carried out using different amounts of adsorbent (2–10 gL⁻¹). The effect of m-WCH and m-OCH amount on MB removal efficiency and adsorption capacity is shown in Fig. 7. The adsorption efficiencies of both adsorbents increased with the increasing amount of biomass, and there was no significant change in MB removal efficiencies after a certain amount. When the amount of m-WCH was increased from 2 to 6 gL⁻¹, the MB removal efficiency increased from 11 to 93%, and the adsorption capacity (q_e) increased from 5.54 to 15.41 mg g⁻¹. When the amount of m-WCH was increased from 6 to 10 gL⁻¹, the MB removal efficiency increased from 93 to 94%, and the adsorption capacity (q_e) decreased from 15.41 to 8.81 mg g⁻¹. When the amount of m-OCH was increased from 2 to 6 gL⁻¹, the MB removal efficiency increased from 19 to 86%, and the adsorption capacity (q_e) increased from 9.09 to 14.21 mg g⁻¹. When the amount of m-OCH was increased from 6 to 10 gL⁻¹, the MB removal efficiency increased from 86 to 89%, and the adsorption capacity (q_e)

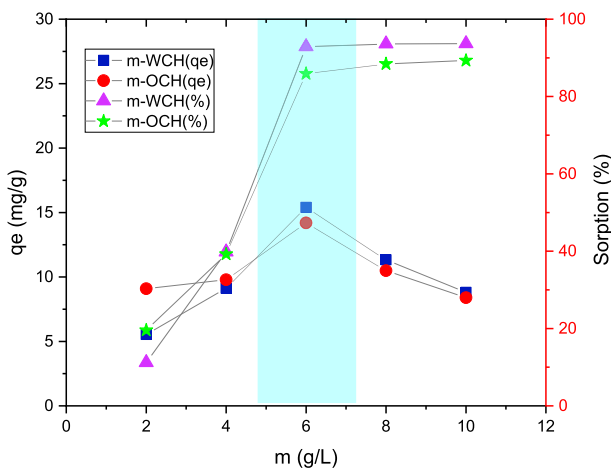


Fig. 7 Influence of m-WCH and m-OCH dosage on MB removal efficiency and uptake

decreased from 14.21 to 8.39 mg g⁻¹. The reason for the increase in MB removal efficiency and decrease in q_e value is the decrease in the amount of MB retained by the unit adsorbent due to the increase in the available binding areas of the adsorbent, in other words, the free adsorption areas [89]. According to the results obtained, MB for m-WCH and m-OCH. For removal, adsorption amounts were chosen as 6 gL⁻¹.

Effect of contact time

The contact time effect on the removal of MB molecules with m-WCH and m-OCH composites was examined in the range of 5–360 min. In order to examine at what rate the adsorption performance changes over time, a t - q_t graph was first drawn, as seen in Fig. 8. It is seen that the adsorption capacity increases with increasing contact time for both adsorbents. Thanks to the large usable surface area during MB removal, the removal rate increased rapidly in the first stage. The removal rate slowed down in the time period from the beginning of saturation of the adsorbent surface area until equilibrium was reached [89]. The possible reason for this increase is the formation of a high repulsive force between the adsorbents at high initial concentration and the adsorbents in the water environment, thus increasing the diffusion rate [90]. Due to the gradual filling of the pores by the adsorbents, the rapidly increasing adsorption capacity slowed down and almost reached equilibrium [91]. In the use of m-WCH composite, 1.60 mg g⁻¹ removal was achieved in the first 5 min, while by increasing the contact time, 11.91 mg g⁻¹ removal was achieved at 120 min. In the use of m-OCH composite, 1.57 mg g⁻¹ removal was achieved in the first 5 min, while by increasing the contact time, 13.21 mg g⁻¹ removal was achieved at 120 min. As can be seen here, the adsorption process reaches equilibrium after almost 120 min for all adsorbents. There was no significant change in removal efficiency after 120 min. Equilibrium time was determined as 120 min.

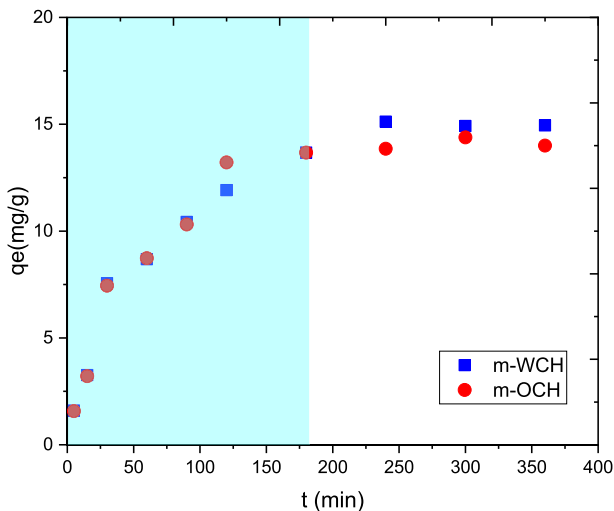


Fig. 8 Effect of contact time on MB adsorption onto m-WCH and m-OCH

Similar results have been previously reported in the literature with different adsorbents used in MB removal. For example, the contact time in MB removal was determined by Mashkoo et al. magnetized chitosan nanocomposite for 180 min [83], Singh et al. determined the contact time for ginkgo biloba as 100 min [33], Krishni et al. determined the contact time for banana leaves as 120 min [92], Han et al. determined the contact time for fallen phoenix tree's leaves as 150 min [93], Sha-koor et al. determined the contact time for citrus limetta peel waste as 180 min [94], Han et al. determined the contact time for lotus leaf as 240 min [95].

Kinetic studies

Adsorption kinetics is a theoretical basis that determines the time required for adsorption equilibrium to be established. Many kinetic models have been developed to detect the mechanisms of an adsorption, such as mass transfer and chemical reaction. Therefore, in order to evaluate the adsorption of m-WCH and m-OCH, the experimental data were verified using pseudo-first-order, pseudo-second-order, an elovich kinetic, and an intraparticle diffusion model (Supplementary Fig. 9). Kinetic variables in the adsorption of MB onto m-WCH and m-OCH are given in Table 6. The theoretical adsorption capacity close to the value determined by experiments and high R^2 values indicate that the pseudo-second-order kinetic model fits better with the adsorption kinetics of m-WCH and m-OCH. According to the pseudo-second-order kinetic model, the adsorption process involves various mechanisms in which chemical and electrostatic interactions occur between functional groups on the adsorbent surface and adsorbate molecules [96]. In this study, the pseudo-second-order kinetic model can say that there are electrostatic interactions between the adsorbent (m-WCH and m-OCH) surface and MB molecules. In addition, it was determined that chemical adsorption was the primary regulating mechanism for adsorption [54]. It was observed that Elovich kinetic model can adequately represent the adsorption of MB onto both the adsorbents based on the regression analysis (Table 6, Supplementary Fig. 9). On the basis of the excellent fitting of both the pseudo-second-order and Elovich model, it can be proposed that the predominant sorption mechanism may be chemisorption. Based on the results of the analysis of the possibility of intraparticle diffusion resistance to influence and control the adsorption process as a rate control stage, to probability looks relatively high, as evidenced by the R^2 value. In addition, the absence of a multi-linear shape in the plot curve $t^{0.5}$ versus qt , implying that the adsorption process controlled by two or more mechanisms has a low probability [97]. Similar results in the study of kinetics with the intraparticle diffusion model have also been stated in previous reports [46].

Effect of temperature

Another important parameter in adsorption studies is the temperature of the adsorption medium. The effect of temperature on the removal of MB molecules with m-WCH and m-OCH adsorbents was investigated by adsorption studies performed at different temperatures (25 °C, 35 °C, 45 °C and 55 °C) and relevant

Table 6 Kinetic model parameter for the adsorption of MB onto m-WCH and m-OCH

Kinetics modeling	Parameters	C_o (ppm)	Adsorbent		
			m-WCH	m-OCH	
Pseudo first-order	$q_{e_{exp}}$	50	8.02	7.89	
		100	15.57	14.73	
		150	23.22	21	
	k_1	50	0.0099	0.009	
		100	0.0098	0.0096	
		150	0.0147	0.0129	
	q_e	50	7.26	6.27	
		100	11.96	9.63	
		150	22.13	16.22	
	R^2	50	0.981	0.923	
		100	0.914	0.869	
		150	0.966	0.923	
	Pseudo second-order	k_2	50	0.0012	0.0014
			100	0.001	0.0013
			150	0.0007	0.0006
q_e		50	9.86	9.43	
		100	17.57	16.31	
		150	26.88	25.64	
R^2		50	0.991	0.99	
		100	0.994	0.992	
		150	0.985	0.971	
Elovich		α	50	0.329	0.337
			100	0.865	0.904
			150	1.377	1.069
	β	50	0.522	0.534	
		100	0.289	0.303	
		150	0.19	0.193	
	R^2	50	0.965	0.96	
		100	0.977	0.961	
		150	0.944	0.955	
	Intraparticle diffusion	k_{id}	50	0.456	0.444
			100	0.812	0.758
			150	1.244	1.191
C		50	0.142	0.244	
		100	1.683	2.083	
		150	2.736	1.78	
R^2		50	0.929	0.918	
		100	0.913	0.859	
		150	0.889	0.858	

Table 7 Thermodynamic parameters for the adsorption of MB molecules on m-WCH and m-OCH

Adsorbent	ΔS° (J K ⁻¹ mol ⁻¹)	ΔH° J mol ⁻¹	ΔG° (J mol ⁻¹)				R^2
			$T=298.15$ K	$T=308.15$ K	$T=318.15$ K	$T=328.15$ K	
m-WCH	-90.59	-33212.19	-6202.31	-5296.39	-4390.48	-3484.56	0.977
m-OCH	-120.01	-40277.85	-4496.78	-3296.68	-2096.58	-896.47	0.991

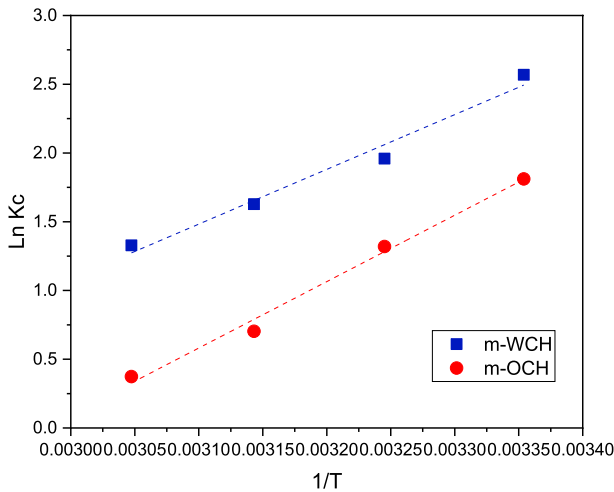


Fig. 9 Thermodynamics plot for the adsorption of MB

results were obtained (Supplementary Fig. 10). With increasing temperature, the diffusion rate of MB molecules toward the adsorbent pores increases depending on the density of the solution. In addition, temperature change also affects the equilibrium capacity of the adsorption process. The adsorption process is generally exothermic, and the adsorption capacity increases with decreasing temperature. As a result of these studies, no significant change was observed in the adsorption capacities of m-WCH and m-OCH adsorbents caused by the temperature difference. However, in the results obtained, it was observed that as the temperature increased, the adsorption capacity was higher at low temperatures. Therefore, experimental studies were carried out at 25 °C.

Thermodynamics study

The effect of temperature on the adsorption of MB molecules was investigated using m-WCH and m-OCH, and the thermodynamic constants calculated with the obtained data are given in Table 7. Free energy change values (ΔG°) were calculated from the relationship in Eqs. 17, 18.

$$\Delta G^\circ = -RT \ln K_c \quad (17)$$

$$\ln K_c = \frac{\Delta S^\circ}{R} - \frac{\Delta H^\circ}{RT} \quad (18)$$

In this study, the thermodynamic parameters (ΔG° , ΔH° , ΔS°) of the experimental studies were determined (Fig. 9). The fact that ΔH° , one of the thermodynamic parameters calculated for the removal of m-WCH and m-OCH and MB molecules, is negative shows that the processes are exothermic [61]. Melo et al. [98] explained the reason for the decrease in adsorption capacity at high temperatures and suggested that this could be explained by three main reasons: (i) high temperature of the environment increases the solubility of MB molecules, which prevents adsorption from the solvent-adsorbate interaction. (ii) the adsorbent-adsorbate interaction weakens due to the high kinetic energy coming from the environment; and (iii) the mobility of MB in solution increases, thus affecting the adsorption kinetics. The negative value of ΔS° indicates that the disorder at the interface between adsorbance (m-WCH and m-OCH) and MB decreases during the adsorption process [99]. Negative ΔG° values indicate that MB adsorption occurs thermodynamically spontaneously and naturally on m-WCH and m-OCH. Additionally, the decrease of ΔG° with increasing temperature indicates that the MB adsorption process occurs more at higher temperatures.

Results supporting our results have been seen in the literature. For example, Zein et al., it was reported that the MB adsorption process of biowaste lemongrass leaves was spontaneous and exothermic [76]. They suggested that the adsorption of MB by lemongrass leaves proceeds through electrostatic attraction, cationic exchange, π - π bonding, and hydrogen bonding. Liu et al. prepared new bio-adsorbent via one-step cross-linking using agricultural waste, CoFe_2O_4 , and chitosan as raw materials for the adsorption of MB and suggested that the adsorption was a spontaneous, exothermic, and randomness reduction process [100].

Effect of pH

One of the most important parameters in the adsorption of organic dyes is the pH of the environment. Because the pH of the solution determines the active binding sites, surface charge and ionization degree on the adsorbent surface. The pH type of the solution causes competition between H^+ and OH^- ions and the composite adsorbent for the binding sites of the composite adsorbent and affects the adsorption capacity and removal rate [89, 90, 101]. On the m-WCH and m-OCH adsorbents of MB solutions to investigate the adsorption behavior, adsorption experiments were carried out at different pH values and the results are shown in Fig. 10. According to Fig. 10, it is possible to confirm that MB adsorption largely depends on pH. When Fig. 10 is examined, the highest adsorption efficiency was achieved for MB with m-WCH adsorbent at pH 6. At higher pH values, no significant change was observed in the MB removal efficiency of the adsorbent. On the other hand, when Fig. 10 is examined, the highest adsorption efficiency was achieved for MB at pH 6 with the

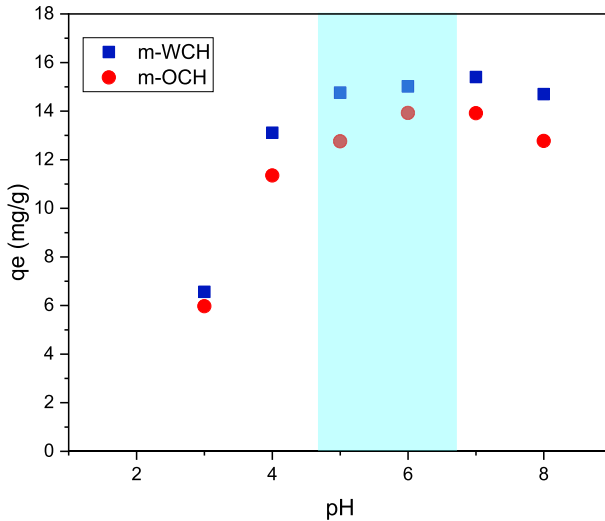


Fig. 10 The effect of pH on adsorption MB with m-WCH and m-OCH

m-OCH adsorbent. At higher pH values, no significant change was observed in the MB removal efficiency of the adsorbent. For this reason, subsequent studies were carried out at pH 6. The observed increase in adsorption capacity with increasing pH is explained by the deprotonation of the binding sites on the adsorbent surface and thus the increase in the negative charge density on the surface. Thus, there is an electrostatic interaction between the negatively charged adsorbent and MB molecules [89]. Functional groups such as OH and $-\text{NH}-$ are protonated to form OH_2^+ and $-\text{NH}_2^+$ at low pH, resulting in decreased binding ability of MB. The strong electrical repulsion between the positively charged surface and the MB prevents the MB from coming into contact with the adsorbent. With increase in pH, functional groups gradually deprotonate. In this case, the adsorbent gains rebinding ability and its removal capacity increases with increasing solution pH. Similar results have also been found in the literature. Sakkayawong et al. [102], the removal of some reactive dyes from aqueous solution with chitosan was examined under acidic and basic conditions. It was observed that in an acidic environment, electrostatic interaction occurred between the dyestuff and functional groups (amino groups) on the chitosan surface, and in a basic environment, covalent bonding occurred between the hydroxyl groups on the chitosan surface and the dyestuff. It has also been stated that only chemical adsorption occurs in acidic conditions, and both physical and chemical adsorption occur in basic conditions. Kumar et al. [103], with the new adsorbent they prepared from chitosan-coated neem flower powder, found that the adsorption of MB from aqueous media increased with increasing dye concentration between pH 6 and 9, and the rate of removal of the dye from the solution increased. In another study, Mustafa used H_2SO_4 cross-linked magnetic chitosan nanocomposite beads to remove MB from aqueous solution [104]. At low pH, the adsorption capacity was increased due to the large amount of H^+ in the solution leading to protonation of the

Table 8 The distribution coefficient (K_d), selectivity coefficient (k) and relative selectivity coefficient (k') for m-WCH and m-OCH

Adsorbent	Dye		K_d	k	k'
m-WCH	MB/MO	MB	2.228	14.151	3.115
		MO	0.157		
m-OCH	MB/MO	MB	0.319	4.543	
		MO	0.070		

active sites of chitosan and the repulsion force arising between the adsorbent and MB. They determined that it was low. It was concluded that by increasing the pH, the H^+ content in the solution decreased and the adsorption capacity increased.

Selectivity study

Adsorption capacities of m-WCH and m-OCH in the presence of competitive ions such as MB/MO was studied in a batch system and the result was presented in Table 8. To investigate and compare the selective adsorption performances for m-WCH and m-OCH composites, the mixture of MO and MB dyes were prepared at pH 6 since the MB adsorption capacity of the composites at high pH is higher than MO adsorption capacity at acidic pH. Table 8. shows that adsorption of MB molecules in the m-WCH was more selective comparing with adsorption MB molecules onto m-OCH even MB exist together with MO as a competitor molecules respectively [47]. K_d value of MB adsorption in the competitive adsorption between MB/MO onto m-WCH was higher than on the m-OCH. The k value of competitive adsorption between MB/MO for m-WCH as adsorbent was greater than m-OCH as adsorbent. The k' value for MB/MO onto m-WCH was much higher than on the m-OCH. Value of k' showed that adsorption of MB dye molecules onto m-WCH in the competitive adsorption between MB/MO system is 3.115 times larger than onto m-OCH. The result proves that the m-WCH has a very high selectivity degree to adsorption the MB ion even MO exist together in sample solution.

Adsorption mechanism of methylene blue dye

The mechanism of MB removal from water using composite adsorbents involves many complex interactions between MB and adsorbent. Existing literature leads us to the conclusion that adsorption involves multiple mechanisms working together, some dominant and others dependent on the prevailing conditions of the system. According to the literature, the adsorption of MB by hydrogels relies on four mechanisms: electrostatic interactions, hydrogen-bond interactions, π - π interactions and hydrophobic interactions [105–107]. The active groups of the m-WCH and m-OCH composite are capable of adsorbing cationic contaminants since the adsorbent is comprised of chitosan and WL or OL, both of which naturally contain abundant active groups. To elucidate the interactions between m-WCH or m-OCH and MB and evaluate their adsorption mechanisms, we performed FTIR tests to reveal the changes of different functional groups and peak positions. A comparison of the

survey FTIR spectra (Fig. 4) revealed that after the adsorption, new peaks were present; the appearance of peaks characteristic of MB and the displacement of peaks also changed [108]. The active groups of m-WCH or m-OCH having negative surface charges in basic media interact electrostatically with the positive group of the MB dye. The H-atom sites located on the surface of m-WCH or m-OCH, which interact with the nitrogen in the structure of the MB dye, probably serve as a vital element for the adsorption of MB. In addition, specifically, hydrogen bond interactions occur between N/S in MB molecules and –OH groups in m-WCH or m-OCH [109]. The hydrophobic regions of the MB molecules can interact with the hydrophobic regions of the chitosan chains (e.g., –CH₃ groups) through hydrophobic interactions [110]. In addition, the role of pores and the π – π interaction between the benzene ring in the MB molecule and the hexagonal skeleton of the adsorbent might also make important contributions to the adsorption [111]. Chitosan contains acetyl groups (–COCH₃) attached to amino groups, further increasing its adsorption properties against MB dye [112]. These combined interaction mechanisms, including hydrogen bonding, electrostatic interactions, and π – π interactions, acted together in the adsorption process between m-WCH or m-OCH and MB, leading to excellent performance in dye removal (Fig. 11).

Recycling efficiency

Reusability of adsorbents is an important factor in determining economic and environmental efficiency. Reusability makes the adsorption process more economical by both eliminating the dependence of the process on the supply of the adsorbent used

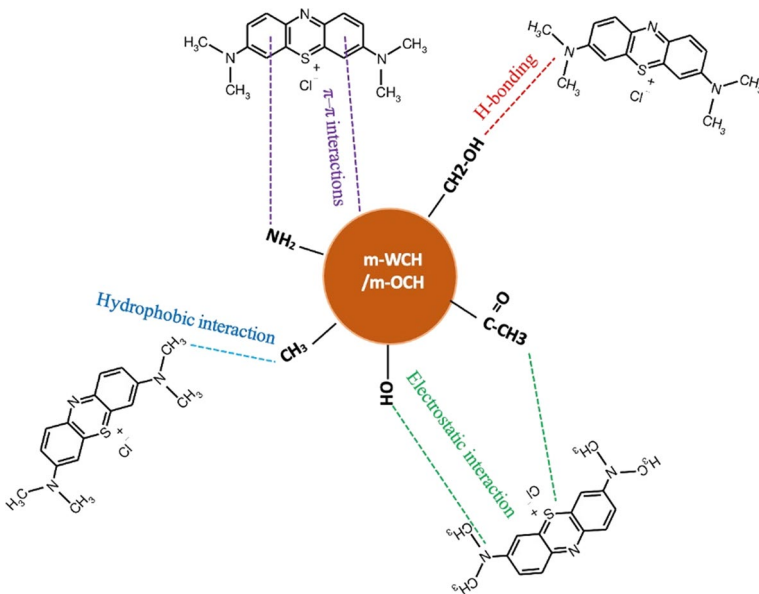


Fig. 11 Mechanism of adsorption of MB onto m-WCH and m-OCH showing different interactions

and reducing process costs [60]. A series of desorption experiments were performed with 1% HCl to determine the reusability and efficiency of m-WCH and m-OCH in MB adsorption (Supplementary Fig. 11). First, composite adsorbents saturated with 1 g/L MB were placed in 50 mL of desorption medium (1% HCl) and continuously shaken in the shaker at 150 rpm for one hour. Then the composite adsorbent was filtered and washed with distilled water. In order to investigate the reuse of m-WCH and m-OCH, 5-cycle adsorption–desorption processes were applied and it was determined that the adsorption capacity decreased only by 8% and 12% for MB. It can be emphasized that there was a slight decrease in the adsorption capacity of the composite beads prepared in this study after 5 adsorption–desorption cycles, therefore they have a stable use potential.

Conclusions

The amount and variety of industrial waste in the world is increasing day by day. Food industry waste is an important group that contains valuable substances in its structure and has the potential to turn into valuable substances. Olive waste/by-products, which are frequently used in olive oil production around the world, and walnut production waste/by-products, which are frequently used in different sectors such as food, have the potential to both prevent environmental pollution and contribute to the economy of countries when used correctly. On the other hand, the main reason for the use of biobased polymers in any application is their environmentally friendly advantages along with easy accessibility, biodegradability, and low cost. For these reasons, composite adsorbents were synthesized together with plant wastes using chitosan as a biopolymer in composite synthesis to be used in MB removal. FTIR, SEM, EDX and XRD analyzes were carried out within the scope of characterization of adsorbents. pH and zero charge point values play an important role in adsorption results. The pH_{PZC} values for m-WCH and m-OCH were 5.2 and 5.5 respectively. The most suitable pH for MB adsorption efficiency in the batch system was found to be 6. On the other hand, the optimum adsorbent dosage for the removal of m-WCH, m-OCH and MB molecules from the aqueous medium was found to be 6 gL^{-1} . From the R^2 values obtained for the kinetic models for both adsorbents, it was found that the most appropriate model was the pseudo-second-order kinetic model. The effect of the initial MB concentration was also examined and the results obtained were evaluated with different isotherm models. When the R^2 values of the isotherm models for m-WCH and m-OCH were compared, it was found that MB adsorption was compatible with the Langmuir isotherm model. Adsorption capacities were found to be 85.47 mg g^{-1} for m-WCH and 53.48 mg g^{-1} for m-OCH. Additionally, the results showed that walnut leaves and olive leaves can be used as an easily accessible natural adsorbent source. Comparison of the results obtained from MB removal studies with m-WCH and m-OCH composites with the literature is given in Table 5. The adsorption selectivity test using MO as interfering ions shows that the m-WCH material has a very high selectivity to MB compared to m-OCH. It has been observed that the synthesized composites have a usable potential in MB removal. These plant-based adsorbents have shown significant promise in treating wastewater

from different types of industries. We believe that this article will be important in completing the shortcomings of the textile industry in terms of wastewater treatment, as the physical and chemical changes in water harm aquatic creatures and partially negatively affect the ecological order and threaten human and living health, and we hope that it will shed light on future studies.

Supplementary Information The online version contains supplementary material available at <https://doi.org/10.1007/s00289-024-05164-6>.

Funding Open access funding provided by the Scientific and Technological Research Council of Türkiye (TÜBİTAK).

Open Access This article is licensed under a Creative Commons Attribution 4.0 International License, which permits use, sharing, adaptation, distribution and reproduction in any medium or format, as long as you give appropriate credit to the original author(s) and the source, provide a link to the Creative Commons licence, and indicate if changes were made. The images or other third party material in this article are included in the article's Creative Commons licence, unless indicated otherwise in a credit line to the material. If material is not included in the article's Creative Commons licence and your intended use is not permitted by statutory regulation or exceeds the permitted use, you will need to obtain permission directly from the copyright holder. To view a copy of this licence, visit <http://creativecommons.org/licenses/by/4.0/>.

References

1. Papadopoulou K, Kalagona IM, Philippoussis A, Rigas F (2013) Optimization of fungal decolorization of azo and anthraquinone dyes via Box-Behnken design. *Int Biodeterior Biodegr* 77:31–38
2. Neolaka YA, Riwu AA, Aigbe UO, Ukhurebor KE, Onyancha RB, Darmokoeseomo H, Kusuma HS (2023) Potential of activated carbon from various sources as a low-cost adsorbent to remove heavy metals and synthetic dyes. *Results Chem* 5:100711
3. Islam T, Repon MR, Islam T, Sarwar Z, Rahman MM (2023) Impact of textile dyes on health and ecosystem: a review of structure, causes, and potential solutions. *Environ Sci Pollut Res* 30(4):9207–9242
4. Chequer FMD, Lizier TM, de Felício R, Zanoni MVB, Deboni HM, Lopes NP, Oliveira DP (2011) analyzes of the genotoxic and mutagenic potential of the products formed after the biotransformation of the azo dye disperse red 1. *Toxicol in Vitro* 25(8):2054–2063
5. Ravikumar K, Deebika B, Balu K (2005) Decolorization of aqueous dye solutions by a novel adsorbent: application of statistical designs and surface plots for the optimization and regression analysis. *J Hazard Mater* 122(1–2):75–83
6. Sun L, Hu D, Zhang Z, Deng X (2019) Oxidative degradation of methylene blue via PDS-based advanced oxidation process using natural pyrite. *Int J Environ Res Public Health* 16(23):4773
7. Cheng J, Zhan C, Wu J, Cui Z, Si J, Wang Q, Peng X, Turng LS (2020) Highly efficient removal of methylene blue dye from an aqueous solution using cellulose acetate nanofibrous membranes modified by polydopamine. *ACS Omega* 5(10):5389–5400
8. Sheynkin YR, Starr C, Li PS, Goldstein M (1999) Effect of methylene blue, indigo carmine, and renografin on human sperm motility. *Urology* 53(1):214–217
9. Tan IAW, Ahmad AL, Hameed BH (2008) Adsorption of basic dye using activated carbon prepared from oil palm shell: batch and fixed bed studies. *Desalination* 225(1–3):13–28
10. Contreras M, Grande-Tovar CD, Vallejo W, Chaves-López C (2019) Bio-removal of methylene blue from aqueous solution by *Galactomyces geotrichum* KL20A. *Water* 11(2):282
11. International Agency for Research on Cancer (1997) IARC monographs on the evaluation of carcinogenic risks to humans. Polychlorinated dibenzo-para-dioxins and polychlorinated dibenzofurans

12. Hassan MM, Carr CM (2018) A critical review on recent advancements of the removal of reactive dyes from dyehouse effluent by ion-exchange adsorbents. *Chemosphere* 209:201–219
13. Khan I, Saeed K, Zekker I, Zhang B, Hendi AH, Ahmad A, Ahmad S, Zada N, Ahmad H, Shah LA, Shah T, Khan I (2022) Review on methylene blue: Its properties, uses, toxicity and photodegradation. *Water* 14(2):242
14. Mussa ZH, Al-Ameer LR, Al-Qaim FF, Deyab IF, Kamyab H, Chelliapan S (2023) A comprehensive review on adsorption of methylene blue dye using leaf waste as a bio-sorbent: isotherm adsorption, kinetics, and thermodynamics studies. *Environ Monit Assess* 195(8):940
15. Parlayıcı Ş (2023) Green biosorbents based on glutaraldehyde cross-linked alginate/sepiolite hydrogel capsules for methylene blue, malachite green and methyl violet removal. *Polym Bull* 80(3):2457–2483
16. Yar A, Parlayıcı Ş (2022) Carbon nanotubes/polyacrylonitrile composite nanofiber mats for highly efficient dye adsorption. *Colloids Surf A Physicochem Eng Asp* 651:129703
17. Mahajan P, Jaspal D, Malviya A (2023) Adsorption of dyes using custard apple and wood apple waste: a review. *J Indian Chem Soc* 100:100948
18. Parlayıcı Ş (2019) Modified peach stone shell powder for the removal of Cr (VI) from aqueous solution: synthesis, kinetic, thermodynamic, and modeling study. *Int J Phytoremediation* 21(6):590–599
19. Garg VK, Amita M, Kumar R, Gupta R (2004) Basic dye (methylene blue) removal from simulated wastewater by adsorption using Indian rosewood sawdust: a timber industry waste. *Dyes Pigment* 63(3):243–250
20. Shukla A, Zhang Y, Dubey P, Margave JL, Shukla SS (2002) The role of sawdust in the removal of unwanted materials from water. *J Hazard Mater B95(1–2):137–152*
21. Khera RA, Iqbal M, Ahmad A, Hassan SM, Nazir A, Kausar A, Kusuma HS, Niasr J, Masood N, Younas U, Nawaz R, Khan MI (2020) Kinetics and equilibrium studies of copper, zinc, and nickel ions adsorptive removal on to *Archontophoenix alexandrae*: conditions optimization by RSM. *Desalin Water Treat* 201:289–300
22. Kuncoro EP, Isnadina DRM, Darmokoesoemo H, Fauziah OR, Kusuma HS (2018) Characterization, kinetic, and isotherm data for adsorption of Pb²⁺ from aqueous solution by adsorbent from mixture of bagasse-bentonite. *Data Br* 16:622–629
23. Kuncoro EP, Soedarti T, Putranto TWC, Darmokoesoemo H, Abadi NR, Kusuma HS (2018) Characterization of a mixture of algae waste-bentonite used as adsorbent for the removal of Pb²⁺ from aqueous solution. *Data Br* 16:908–913
24. Akkaya G, Güzel F (2014) Application of some domestic wastes as new low-cost biosorbents for removal of methylene blue: kinetic and equilibrium studies. *Chem Eng Commun* 201(4):557–578
25. Belala Z, Jeguirim M, Belhachemi M, Addoun F, Trouvé G (2011) Biosorption of basic dye from aqueous solutions by date stones and palm-trees waste: kinetic, equilibrium and thermodynamic studies. *Desalination* 271(1–3):80–87
26. Mekuria D, Diro A, Melak F, Asere TG (2022) Adsorptive removal of methylene blue dye using biowaste materials: barley bran and enset midrib leaf. *J Chem*. <https://doi.org/10.1155/2022/4849758>
27. Mousavi SA, Mahmoudi A, Amiri S, Darvishi P, Noori E (2022) Methylene blue removal using grape leaves waste: optimization and modeling. *Appl Water Sci* 12(5):1–11
28. Halysh V, Sevastyanova O, Pikus S, Dobelev G, Pasalskiy B, Gun'ko VM, Kartel M, (2020) Sugar-cane bagasse and straw as low-cost lignocellulosic sorbents for the removal of dyes and metal ions from water. *Cellulose* 27(14):8181–8197
29. Nithyalakshmi B, Saraswathi R (2023) Removal of colorants from wastewater using biochar derived from leaf waste. *Biomass Convers Biorefin* 13:311–327
30. Hameed BH, Mahmood DK, Ahmad AL (2008) Sorption equilibrium and kinetics of basic dye from aqueous solution using banana stalk waste. *J Hazard Mater* 158(2–3):499–506
31. Hameed BH, El-Khaiary MI (2008) Removal of basic dye from aqueous medium using a novel agricultural waste material: pumpkin seed hull. *J Hazard Mater* 155(3):601–609
32. Mahadlek J, Mahadlek J (2020) Investigation of various factors affecting methylene blue adsorption on agricultural waste: Banana stalks. *Sci Eng Health Stud* 14:47–61
33. Singh R, Singh TS, Odiyo JO, Smith JA, Edokpayi JN (2020) Evaluation of methylene blue sorption onto low-cost biosorbents: equilibrium, kinetics, and thermodynamics. *J Chem* 2020:8318049
34. Rodriguesa F, Pimentela FB, Oliveiraa MB (2015) Olive by-products: challenge application in cosmetic industry. *Ind Crops Prod* 70:116–124

35. Bou Abdallah I, Baatour O, Mechrgui K, Herchi W, Albouchi A, Chalghoum A, Boukhchina S (2016) Essential oil composition of walnut tree (*Juglans regia* L.) leaves from Tunisia. *J Essent Oil Res* 28(6):545–550
36. Jahanban-Esfahlan A, Ostadrahimi A, Tabibiazar M, Amarowicz R (2019) A comparative review on the extraction, antioxidant content and antioxidant potential of different parts of walnut (*Juglans regia* L.) fruit and tree. *Molecules* 24(2133):1–40
37. Espeso J, Isaza A, Lee JY, Sörensen PM, Jurado P, Avena-Bustillos RJ, Olaizola M, Arboleya JC (2021) Olive leaf waste management. *Front Sustain Food Syst* 5:1–13
38. Pehlivan E, Parlayıcı Ş (2021) Fabrication of a novel biopolymer-based nanocomposite (nano-TiO₂-chitosan-plum kernel shell) and adsorption of cationic dyes. *J Chem Technol Biotechnol* 96(12):3378–3387
39. Mohrazi A, Ghasemi-Fasaei R (2023) Removal of methylene blue dye from aqueous solution using an efficient chitosan-pectin bio-adsorbent: kinetics and isotherm studies. *Environ Monit Assess* 195(2):339
40. Zhang Z, Abidi N, Lucia L (2023) Smart superabsorbent alginate/carboxymethyl chitosan composite hydrogel beads as efficient biosorbents for methylene blue dye removal. *J Mater Sci Technol* 159:81–90
41. Kazemi MS, Sobhani A (2023) CuMn₂O₄/chitosan micro/nanocomposite: green synthesis, methylene blue removal, and study of kinetic adsorption, adsorption isotherm experiments, mechanism and adsorbent capacity. *Arab J Chem* 16(6):104754
42. Chakrabarty T, Kumar M, Shahi VK (2010) Chitosan-based membranes for separation, pervaporation and fuel cell applications: recent developments. *Biopolymers* 10:201–226
43. Demarchi CA, Campos M, Rodrigues CA (2013) Adsorption of textile dye reactive red 120 by the chitosan–Fe (III)-crosslinked: batch and fixed-bed studies. *J Environ Chem Eng* 1(4):1350–1358
44. Parlayıcı Ş, Pehlivan E (2019) Fast decolorization of cationic dyes by nano-scale zero valent iron immobilized in sycamore tree seed pod fibers: kinetics and modeling study. *Int J Phytoremediation* 21(11):1130–1144
45. Budiana IGMN, Jasman J, Neolaka YA, Riwu AA, Elmsellem H, Darmokoesoemo H, Kusuma HS (2021) Synthesis, characterization and application of cinnamoyl C-phenylcalix [4] resorcinarene (CCPCR) for removal of Cr (III) ion from the aquatic environment. *J Mol Liq* 324:114776
46. Neolaka YA, Lawa Y, Naat JN, Riwu AAP, Darmokoesoemo H, Supriyanto G, Holdsworth CI, Amenaghawon AN, Kusuma HS (2020) A Cr (VI)-imprinted-poly (4-VP-co-EGDMA) sorbent prepared using precipitation polymerization and its application for selective adsorptive removal and solid phase extraction of Cr (VI) ions from electroplating industrial wastewater. *React Funct Polym* 147:104451
47. Neolaka YA, Supriyanto G, Kusuma HS (2018) Adsorption performance of Cr (VI)-imprinted poly (4-VP-co-MMA) supported on activated Indonesia (Ende-Flores) natural zeolite structure for Cr (VI) removal from aqueous solution. *J Environ Chem Eng* 6(2):3436–3443
48. Dhankhar R, Hooda A (2011) Fungal biosorption—an alternative to meet the challenges of heavy metal pollution in aqueous solutions. *Environ Technol* 32:467–491
49. Tan LN, Nguyen NCT, Trinh AMH, Do NH, Le KA, Le PK (2023) Eco-friendly synthesis of durable aerogel composites from chitosan and pineapple leaf-based cellulose for Cr (VI) removal. *Sep Purif Technol* 304:122415
50. Alizadeh N, Shariati S, Besharati N (2017) Adsorption of crystal violet and methylene blue on azolla and fig leaves modified with magnetite iron oxide nanoparticles. *Int J Environ Res* 11:197–206
51. Dubinin M, Radushkevich L (1947) Equation of the characteristic curve of activated charcoal. *Chem Zentr* 1(1):875
52. Lagergren S, Svenska BK (1898) About the theory of so-called adsorption of soluble substances. *Vetensk Handl* 24(4):1–39
53. Ho YS, McKay G (1999) Pseudo-second order model for sorption processes. *Process Biochem* 34(5):451–465
54. Neolaka YA, Lawa Y, Naat J, Lalang AC, Widyaningrum BA, Ngasu GF, Niga KA, Darmokoesoemo H, Iqbal M, Kusuma HS (2023) Adsorption of methyl red from aqueous solution using Bali cow bones (*Bos javanicus domesticus*) hydrochar powder. *Results Eng* 17:100824
55. Aigbe UO, Ukhurebor KE, Onyancha RB, Osibote OA, Darmokoesoemo H, Kusuma HS (2021) Fly ash-based adsorbent for adsorption of heavy metals and dyes from aqueous solution: a review. *J Mater Res Technol* 14:2751–2774

56. McMullan D (1995) Scanning electron microscopy 1928–1965. *Scanning* 17(3):175–185
57. Yao J, Odelius K, Hakkarainen M (2020) Carbonized lignosulfonate-based porous nanocomposites for adsorption of environmental contaminants. *Funct Compos Mater* 1(1):1–12
58. Parlayıcı Ş (2023) Novel chitosan/citric acid modified pistachio shell/halloysite nanotubes cross-linked by glutaraldehyde biocomposite beads applied to methylene blue removal. *Int J Phytoremediation* 26:1–16
59. Ainane T, Khammour F, Talbi M, Elkouali MH (2014) A novel bio-adsorbent of mint waste for dyes remediation in aqueous environments: study and modeling of isotherms for removal of methylene blue. *Orient J Chem* 30(3):1183–1189
60. Mosoarca G, Vancea C, Popa S, Dan M, Boran S (2023) A novel high-efficiency natural biosorbent material obtained from sour cherry (*Prunus cerasus*) leaf biomass for cationic dyes adsorption. *Materials* 16(12):4252
61. Farch S, Yahoum MM, Toumi S, Tahraoui H, Lefnaoui S, Kebir M, Zamouche M, Amrane A, Zhang J, Hadadi A, Mouni L (2023) Application of walnut shell biowaste as an inexpensive adsorbent for methylene blue dye: isotherms, kinetics, thermodynamics, and modeling. *Separations* 10(1):60
62. Mahdavi M, Ahmad MB, Haron MJ, Gharayebi Y, Shameli K, Nadi B (2013) Fabrication and characterization of SiO₂/(3-aminopropyl) triethoxysilane-coated magnetite nanoparticles for lead (II) removal from aqueous solution. *J Inorg Organomet Polym Mater* 23(3):599–607
63. El Ghandour H, Zidan H, Khalil MM, Ismail M (2012) Synthesis and some physical properties of magnetite (Fe₃O₄) nanoparticles. *Int J Electrochem Sci* 7(6):5734–5745
64. Panneerselvam P, Morad N, Tan KA (2011) Magnetic nanoparticle (Fe₃O₄) impregnated onto tea waste for the removal of nickel (II) from aqueous solution. *J Hazard Mater* 186(1):160–168
65. Liu R, Yu H, Huang Y (2005) Structure and morphology of cellulose in wheat straw. *Cellulose* 12:25–34
66. Ren Y, Abbood HA, He F, Peng H, Huang K (2013) Magnetic EDTA- modified chitosan/SiO₂/Fe₃O₄ adsorbent: preparation, characterization, and application in heavy metal adsorption. *Chem Eng J* 226:300–311
67. Karimi MH, Mahdavinia GR, Massoumi B, Baghban A, Saraei M (2018) Ionically crosslinked magnetic chitosan/k-carrageenan bioadsorbents for removal of anionic eriochrome black-T. *Int J Biol Macromol* 113:361–375
68. Neolaka YA, Lawa Y, Naat J, Riwu AA, Mango AW, Darmokoeseoemo H, Widyaningrum BA, Iqbal M, Kusuma HS (2022) Efficiency of activated natural zeolite-based magnetic composite (ANZ-Fe₃O₄) as a novel adsorbent for removal of Cr (VI) from wastewater. *J Mater Res Technol* 18:2896–2909
69. Nirmala S, Pasupathy A, Raja T, Raja M (2016) Removal of malachite green from aqueous solutions by adsorption using low cost adsorbent obtained from *Centella asiatica* leaves. *Int J Res Pharm Chem* 6(4):916–921
70. Vanamudan A, Bandwala K, Pamidimukkala P (2014) Adsorption property of rhodamine 6G onto chitosan-g-(*N*-vinyl pyrrolidone)/montmorillonite composite. *Int J Biol Macromol* 69:506–513
71. Adekola FA, Ayodele SB, Yinbor AA (2019) Efficient rhodamine B removal using acid and alkaline-activated *Musa paradisiaca* biochar. *Pol J Environ Stud* 28(5):3063–3070
72. Sevim F, Lacin O, Ediz EF, Demir F (2021) Adsorption capacity, isotherm, kinetic, and thermodynamic studies on adsorption behavior of malachite green onto natural red clay. *Environ Prog Sustain Energ* 40(1):e13471
73. Fan S, Wang Y, Wang Z, Tang J, Tang J, Li X (2017) Removal of methylene blue from aqueous solution by sewage sludge-derived biochar: adsorption kinetics, equilibrium, thermodynamics and mechanism. *J Environ Chem Eng* 5(1):601–611
74. Tran HTT, Hoang LT, Tran HV (2022) Electrochemical synthesis of graphene from waste discharged battery electrodes and its applications to preparation of graphene/Fe₃O₄/chitosan-nanosorbent for organic dyes removal. *Z Anorg Allg Chem* 648(3):e202100313
75. Gupta N, Kushwaha AK, Chattopadhyaya MC (2016) Application of potato (*Solanum tuberosum*) plant wastes for the removal of methylene blue and malachite green dye from aqueous solution. *Arab J Chem* 9:707–716
76. Zein R, Purnomo JS, Ramadhani P, Alif MF, Safni S (2022) Lemongrass (*Cymbopogon nardus*) leaves biowaste as an effective and low-cost adsorbent for methylene blue dyes removal: isotherms, kinetics, and thermodynamics studies. *Sep Sci Technol* 57(15):2341–2357

77. Fiaz R, Hafeez M, Mahmood R (2019) *Ficus palmata* leaves as a low-cost biosorbent for methylene blue: thermodynamic and kinetic studies. *Water Environ Res* 91:689–699
78. Bhattacharyya KG, Sharma A (2005) Kinetics and thermodynamics of methylene blue adsorption on neem (*Azadirachta indica*) leaf powder. *Dyes Pigm* 65:51–59
79. Vadivelan V, Kumar KV (2005) Equilibrium, kinetics, mechanism and process design for the sorption of methylene blue onto rice husk. *J Colloid Interface Sci* 286:90–100
80. Uddin MK, Nasar A (2020) Walnut shell powder as a low-cost adsorbent for methylene blue dye: isotherm, kinetics, thermodynamic, desorption and response surface methodology examinations. *Sci Rep* 10(1):7983
81. Al-Azabi K, Al-Marog S, Abukrain A, Sulyman M (2018) Equilibrium, isotherm studies of dye adsorption onto orange peel powder. *Chem Res J* 3:45–59
82. Zhang W, Li H, Tang J, Lu H, Liu Y (2019) Ginger Straw Waste-derived porous carbons as effective adsorbents toward methylene blue. *Molecules* 24(3):469
83. Mashkoo F, Nasar A, Jeong C (2022) Magnetized chitosan nanocomposite as an effective adsorbent for the removal of methylene blue and malachite green dyes. *Biomass Convers Biorefin*. <https://doi.org/10.1007/s13399-021-02282-3>
84. Zeng L, Xie M, Zhang Q, Kang Y, Guo X, Xiao H, Peng Y, Luo J (2015) Chitosan/organic recortite composite for the magnetic uptake of methylene blue and methyl orange. *Carbohydr Polym* 123:89–98
85. Xiong R, Wang Y, Zhang X, Lu C (2014) Facile synthesis of magnetic nanocomposites of cellulose@ultra-small iron oxide nanoparticles for water treatment. *RSC Adv* 4(43):22632–22641
86. Santosa IK, Rizkiana MF (2023) Adsorption of methylene blue by magnetic activated carbon/chitosan composites prepared from spent coffee grounds: kinetic, equilibrium and thermodynamic study. *J Biobased Chem* 3(1):66–75
87. Djilani C, Zaghdoudi R, Djazi F, Boucekima B, Lallam A, Modarressi A, Rogalski M (2015) Adsorption of dyes on activated carbon prepared from apricot stones and commercial activated carbon. *J Taiwan Inst Chem Eng* 53:112–121
88. Shah I, Adnan R, Ngah WSW, Mohamed N, Taufiq-Yap YH (2014) A new insight to the physical interpretation of activated carbon and iron doped carbon material: sorption affinity toward organic dye. *Bioresour Technol* 160:52–56
89. Mustafa FH, ElRab EKMG, Kamel RM, Elshaarawy RF (2023) Cost-effective removal of toxic methylene blue dye from textile effluents by new integrated crosslinked chitosan/aspartic acid hydrogels. *Int J Biol Macromol* 248:125986
90. Sarkar KK, Majee S, Pathak U, Polepali S, Halder G, Mandal DD, Mandal T (2019) Development of an integrated treatment strategy for removal of ondansetron using simultaneous adsorption, oxidation and bioremediation technique. *J Environ Chem Eng* 7(2):103020
91. Wu FC, Tseng RL, Juang RS (2009) Characteristics of Elovich equation used for the analysis of adsorption kinetics in dye-chitosan systems. *Chem Eng J* 150(2–3):366–373
92. Krishni RR, Foo KY, Hameed BH (2014) Adsorptive removal of methylene blue using the natural adsorbent-banana leaves. *Desalin Water Treat* 52:6104–6112
93. Han R, Zou W, Yu W, Cheng S, Wang Y, Shi J (2007) Biosorption of methylene blue from aqueous solution by fallen phoenix tree's leaves. *J Hazard Mater* 141:156–162
94. Shakoor S, Nasar A (2016) Removal of methylene blue dye from artificially contaminated water using citrus limetta peel waste as a very low cost adsorbent. *J Taiwan Inst Chem Eng* 66:154–163
95. Han X, Wang W, Ma X (2011) Adsorption characteristics of methylene blue onto low cost biomass material lotus leaf. *Chem Eng J* 171:1–8
96. Hassani A, Soltani RDC, Karaca S (2015) Khataee A (2015) Preparation of montmorillonite–alginate nanobiocomposite for adsorption of a textile dye in aqueous phase: Isotherm, kinetic and experimental design approaches. *J Ind Eng Chem* 21:1197–1207
97. Neolaka YA, Lawa Y, Naat J, Riwi AA, Darmokoesoemo H, Widyaningrum BA, Iqbal M, Kusuma HS (2021) Indonesian Kesambi wood (*Schleichera oleosa*) activated with pyrolysis and H₂SO₄ combination methods to produce mesoporous activated carbon for Pb (II) adsorption from aqueous solution. *Environ Technol Innov* 24:101997
98. Melo BC, Paulino FAA, Cardoso VA, Pereira AGB, Fajardo AR, Rodrigues FHA (2018) Cellulose nanowhiskers improve the methylene blue adsorption capacity of chitosan-g-poly(acrylic Acid) hydrogel. *Carbohydr Polym* 181:358–367
99. Kul A, Alacabey İ, Kılıç NÇ (2010) Removal of cobalt ions from aqueous solution by diatomite. *Hacetepce J Biol Chem* 38(2):85–93

100. Liu S, Ge H, Cheng S, Zou Y (2018) Green synthesis of magnetic 3D bio-adsorbent by corn straw core and chitosan for methylene blue removal. *Environ Technol* 41(16):2109–2121
101. Chen K, Du L, Gao P, Zheng J, Liu Y, Lin H (2021) Super and selective adsorption of cationic dyes onto carboxylate-modified passion fruit peel biosorbent. *Front Chem* 9:646492
102. Sakkayawong N, Thiravetyan P, Nakbanpote W (2005) Adsorption mechanism of synthetic reactive dye wastewater by chitosan. *J Colloid Interface Sci* 286(1):36–42
103. Kumar P, Induja S, Raghavan P, Gajalakshmi B, Parthasarathy V (2022) A novel chitosan-coated neem flower bio-adsorbent for the removal of methylene blue dye from wastewater: thermodynamics, isotherm and kinetic studies. *Curr Chem Lett* 11(4):371–382
104. Mustafa I (2019) Methylene blue removal from water using H₂SO₄ crosslinked magnetic chitosan nanocomposite beads. *Microchem J* 144:397–402
105. Sivakumar R, Lee NY (2022) Adsorptive removal of organic pollutant methylene blue using polysaccharide-based composite hydrogels. *Chemosphere* 286:131890
106. Wang H, Li J, Ding N, Zeng X, Tang X, Sun Y, Lei T, Lin L (2020) Eco-friendly polymer nanocomposite hydrogel enhanced by cellulose nanocrystal and graphitic-like carbon nitride nanosheet. *Chem Eng J* 386:124021
107. Mallakpour S, Tabesh F (2021) Green and plant-based adsorbent from tragacanth gum and carboxyl-functionalized carbon nanotube hydrogel bionanocomposite for the super removal of methylene blue dye. *Int J Biol Macromol* 166:722–729
108. Wan X, Rong Z, Zhu K, Wu Y (2022) Chitosan-based dual network composite hydrogel for efficient adsorption of methylene blue dye. *Int J Biol Macromol* 222:725–735
109. Yang P, Lu Y, Zhang H, Li R, Hu X, Shahab A, Elnaggar AY, Alrefaei AF, Almutairi MH, Ali E (2024) Effective removal of methylene blue and crystal violet by low-cost biomass derived from eucalyptus: characterization, experiments, and mechanism investigation. *Environ Technol Innov* 33:103459
110. Ben Amor I, Hemmami H, Laouini SE, Zeghoud S, Benzina M, Achour S, Naseef A, Alsalmeh A, Barhoum A (2023) Use of insect-derived chitosan for the removal of methylene blue dye from wastewater: process optimization using a central composite design. *Materials* 16(14):5049
111. Parlayıcı Ş (2023) Facile preparation of chitosan-coated biomass-based adsorbent beads for effective uptake of methylene blue from aqueous solution. *Biomass Convers Biorefin*. <https://doi.org/10.1007/s13399-023-04065-4>
112. Amor IB, Hemmami H, Laouini SE, Abdelaziz AG, Barhoum A (2023) Influence of chitosan source and degree of deacetylation on antibacterial activity and adsorption of AZO dye from water. *Biomass Convers Biorefin*. <https://doi.org/10.1007/s13399-023-03741-9>

Publisher's Note Springer Nature remains neutral with regard to jurisdictional claims in published maps and institutional affiliations.

Authors and Affiliations

Şerife Parlayıcı¹  · Aslı Aras¹

✉ Şerife Parlayıcı
sparlayici@ktun.edu.tr

¹ Department of Chemical Engineering, Konya Technical University, Campus, 42079 Konya, Turkey